LEADING RESEARCH CENTER ON
QUANTUM COMPUTING

RQC

Quantum computing in the noise environment: variational approach and error correction

Aleksey Fedorov
Russian Quantum Center

Theory: E. Kiktenko (RQC), I. Luchnikov (RQC), M. Sapova (RQC), A. Boev (RQC), A. Antipov (RQC) *et. al.*

LRC collaboration

Industry collaboration: Nissan (Japan), Gero AI (Singpore), Genotek (Russia)

40 years of quantum computing

Yury Manin,
Computable and non-computable (1980)

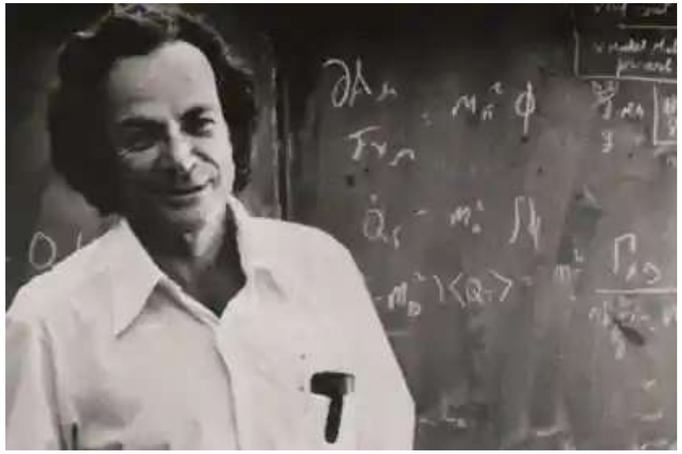

Richard Feynman,
Simulating physics with computers (1981)

Editorial | Published: 10 January 2022

40 years of quantum computing

Nature Reviews Physics **4**, 1 (2022) | Cite this article

3388 Accesses | **21** Altmetric | Metrics

This year we celebrate four decades of quantum computing by looking back at the milestones of the field and forward to the challenges and opportunities that lie ahead.

Quantum computing 40 years later

John Preskill

Forty years ago, Richard Feynman proposed harnessing quantum physics to build a more powerful kind of computer. Realizing Feynman's vision is one of the grand challenges facing 21st century science and technology. In this article, we'll recall Feynman's contribution that launched the quest for a quantum computer, and assess where the field stands 40 years later.

Comments: 49 pages. To appear in Feynman Lectures on Computation, 2nd edition, published by Taylor & Francis Group, edited by Anthony J. G. Hey. (v2) typos corrected
Subjects: **Quantum Physics (quant-ph)**
Cite as: arXiv:2106.10522 **[quant-ph]**
(or arXiv:2106.10522v2 **[quant-ph]** for this version)

40 years of quantum computing: Main challenges

- Physical platform for quantum computing: What can be an analog of a ‘silicon transistor’ for the quantum computing technology?

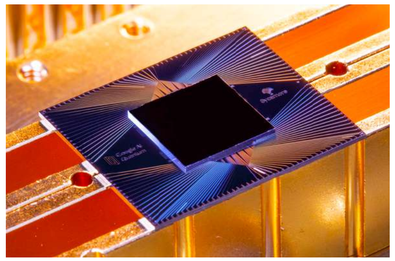
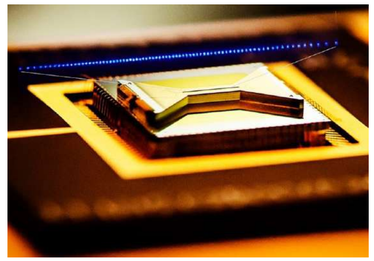
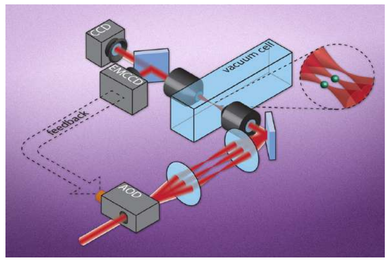

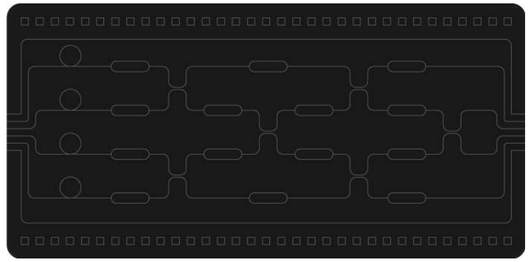

- Efficient error correction: Is it possible to develop efficient error correction techniques and enter the era of fault-tolerant quantum computing? Is it possible to use existing NISQ devices efficiently?

- Quantum algorithms and applications: What are most interesting near-term applications of quantum computing?

How to factor 2048 bit RSA integers in 8 hours using 20 million noisy qubits

Craig Gidney, Martin Ekerå

known approach. By laying out and optimizing the surface-code resources required of our approach we show that FeMoCo can be simulated using about four million physical qubits and under 4 days of runtime, assuming 1-μs cycle times and physical gate-error rates no worse than 0.1%.

C. Gidney and M. Ekerå, How to factor 2048 bit RSA integers in 8 hours using 20 million noisy qubits, arXiv:1905.09749; J. Lee, Even more efficient quantum computations of chemistry through tensor hypercontraction, arXiv:2011.03494.

Origin of a quantum speedup

- “Naive quantum parallelism” (D. Deutsch): Quantum computers solve problems by trying all possible solutions in parallel.

- Access to exponentially large computational spaces: However, such an “access" takes place also for classical systems since N classical bits can take 2^N possible values.

- Quantum complexity (J. Preskill): Quantum information is very different in that writing down a complete description of just one typical configuration of N qubits is complex.

Classical system	Quantum system
A single bit string of n zeros and ones	2^n complex numbers

- Gottesman-Knill theorem: Even some highly entangled states can be simulated efficiently.

Origin of a quantum speedup in the NISQ era

- Role of decoherence: The control of decoherence of a qubit is a central problem of various models of quantum computation, where an incoming qubit is transmitted through a noisy channel.

- Quantum advantage experiments: Is it possible to demonstrate (useful) quantum advantage in the presence of noise?

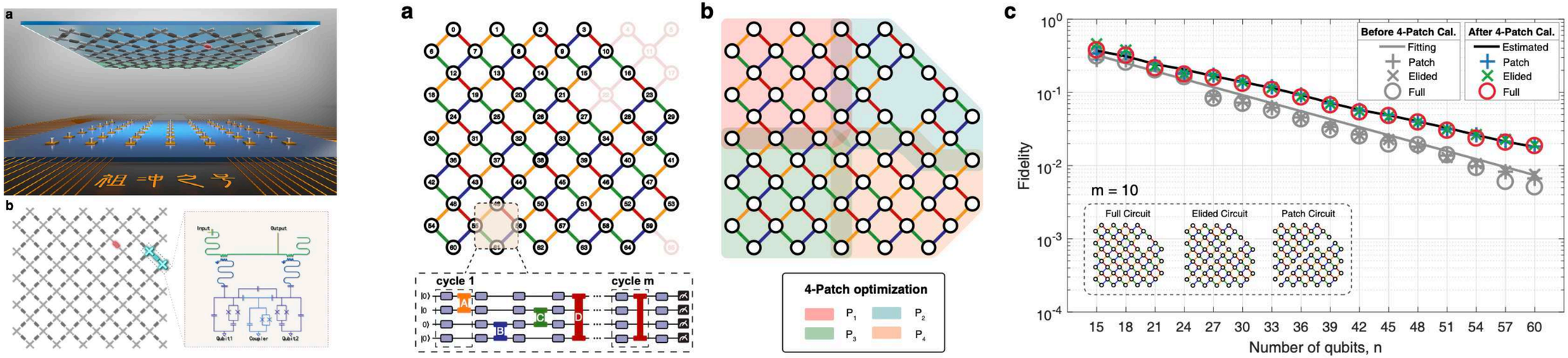

Q. Zhu et al., Quantum Computational Advantage via 60-Qubit 24-Cycle Random Circuit Sampling, https://arxiv.org/abs/2109.03494

Quantum computing applications

- Scientific applications: Use quantum computers to explore new frontiers in science, mainly, physics and computer science.

Quantum phases of matter on a 256-atom programmable quantum simulator

Scaling advantage over path-integral Monte Carlo in quantum simulation of geometrically frustrated magnets

- Specialized applications: random number generation, cryptoanalysis, sampling (?).

How to factor 2048 bit RSA integers in 8 hours using 20 million noisy qubits

Craig Gidney[1] and Martin Ekerå[2]

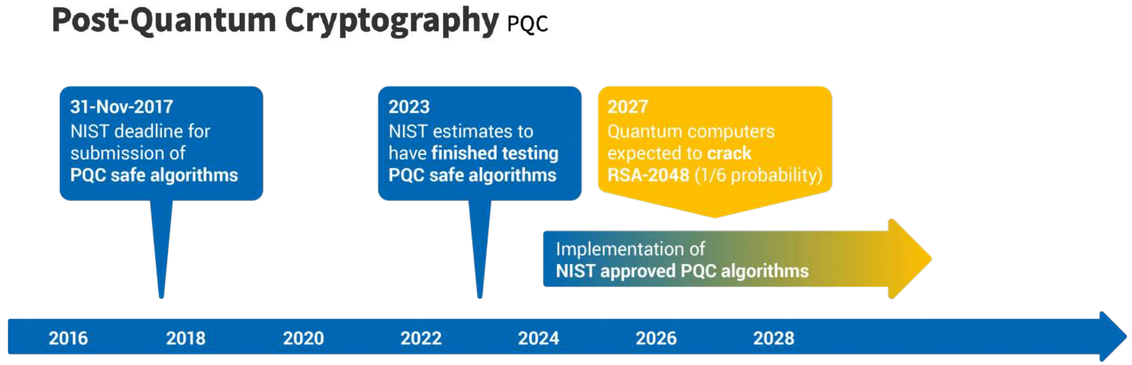

- (Potentially) widespread applications: simulation (quantum and quantum-enhanced), optimization, and machine learning

Quantum computing applications

Simulation

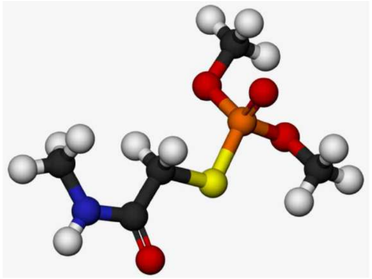

Quantum:
- Chemistry
- Biophysics
- Materials
- Drugs
- …

Classical:
- Linear equations
- Differential equations

Optimization

- Logistics
- Finance
- Job scheduling
- …

Machine learning

- Training networks
- Speed-up linear algebra
- Quantum kernel models

Quantum computing applications: Simulation (chemistry) & Optimization

IONQ: Optimizing electronic structure simulations on a trapped-ion quantum computer using problem decomposition

14 Feb 2021

Simulating a ring of 10 hydrogen atoms without freezing any electrons

https://www.nature.com/articles/s42005-021-00751-9.pdf

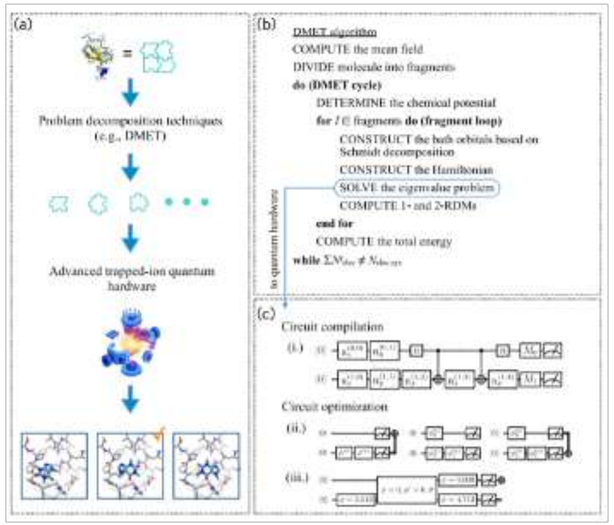

QBoard & Nissan with IBM: Variational quantum eigensolver techniques for simulating carbon monoxide oxidation

25 Aug 2021

Simulating a set of molecules, O2, CO, and CO2, participating in the carbon monoxide oxidation processes.

https://arxiv.org/abs/2108.11167

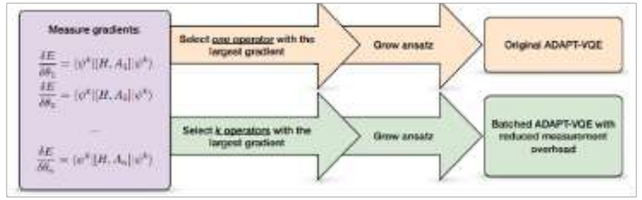

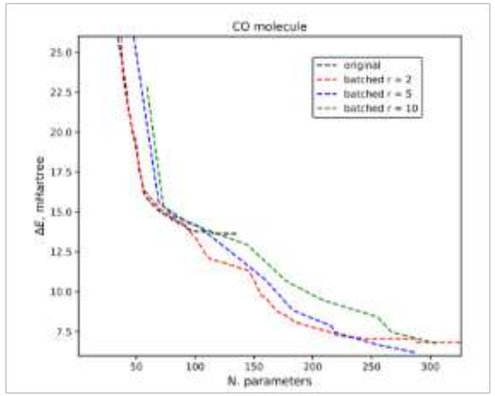

Delta Airlines: Exploring Airline Gate-Scheduling Optimization Using Quantum Computers

18 Nov 2021

One of the many complex problems facing the airline industry today is how to optimize large combinations of cargo and passenger traffic among the planes, gates, personnel and the air traffic flows originating or terminating at an airport

https://arxiv.org/abs/2111.09472

Quantum computing applications: Simulation (chemistry) & Optimization

IBM: Towards Quantum Advantage in Financial Market Risk using Quantum Gradient Algorithms

24 Nov 2021

New estimates for Quantum Advantage for computing Option Greeks – 6,000 qubits, 1MHz speed – 50 times lower than previous best estimates

https://arxiv.org/abs/2111.12509

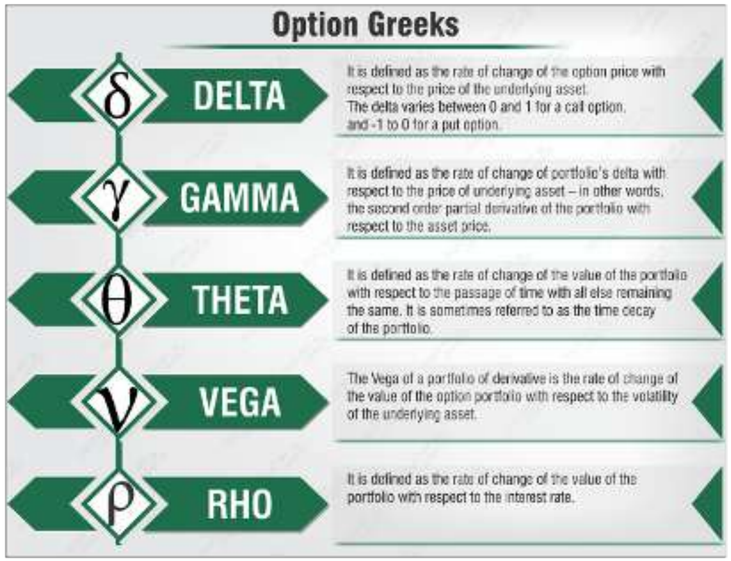

Rigetti Computing: Synthetic weather radar using hybrid quantum-classical machine learning

30 Nov 2021

Quantum kernels can, in principle, perform fundamentally more complex tasks than classical learning machines. The results establish synthetic weather radar as an effective heuristic benchmark for quantum computing capabilities and set the stage for detailed quantum advantage benchmarking on a high-impact operationally relevant problem

https://arxiv.org/abs/2111.15605

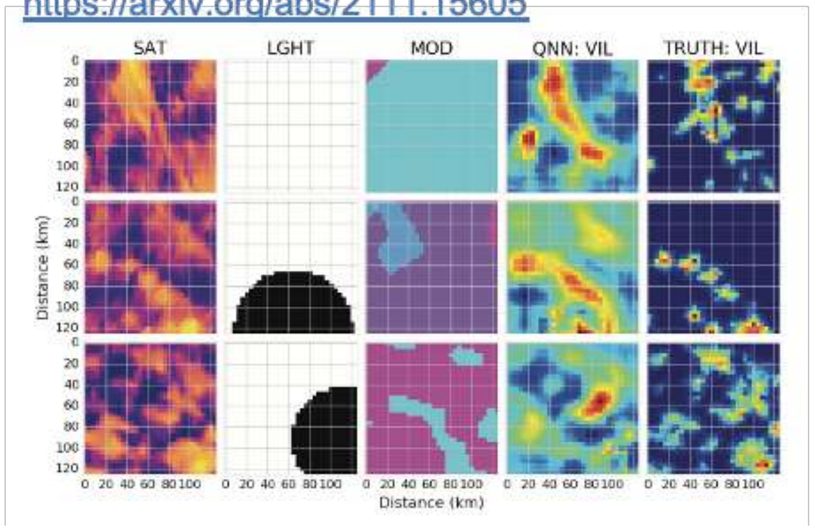

BMW: Quantum Computing Challenge winners

9 Dec 2021

accenture

Sensor Position Optimization
Optimize the setup of the increasing number of sensors for better performance and safety

⟨Q|Q⟩

Pre-production vehicle configuration
Improve the efficiency of the tests of different vehicle components, meeting the safety and performance requirements

Qu & Co

Material deformation in production
Simulate the material response on metal-forming process using discrete element or AI-based solutions to review the producibility

QCWARE

Automated quality assessment
Enhance the objective quality inspection based on ML assessment for defects on vehicle parts produced by metal-forming

Ongoing experiments on error correction: Superconducting circuits

Article

Exponential suppression of bit or phase errors with cyclic error correction

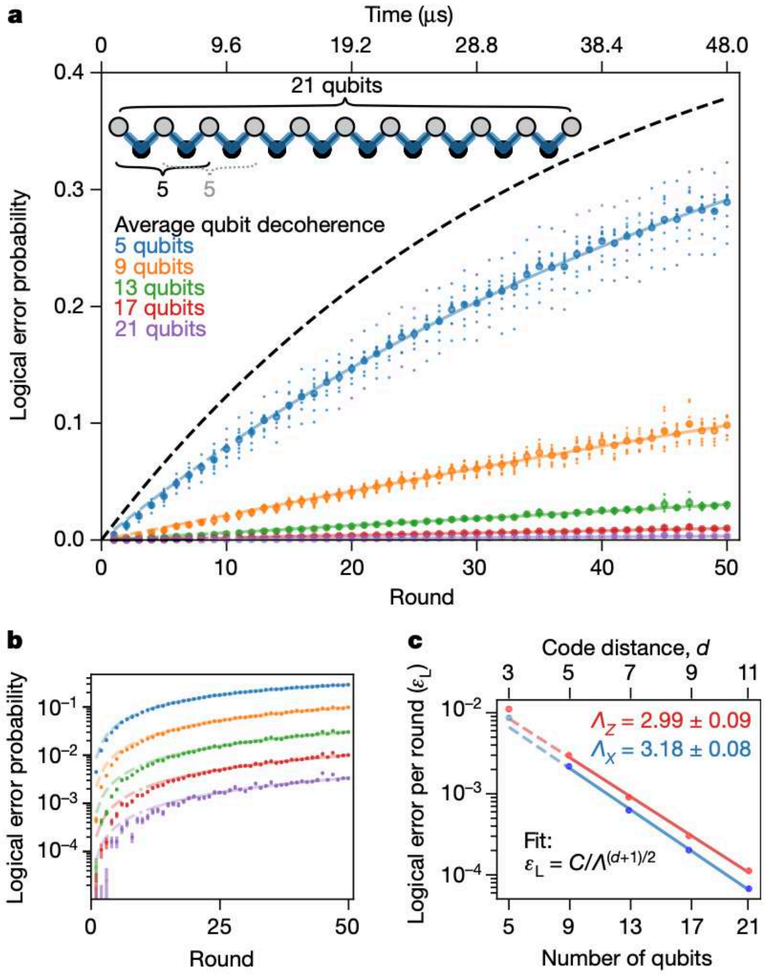

Realization of an Error-Correcting Surface Code with Superconducting Qubits

Youwei Zhao,[1,2,3,*] Yangsen Ye,[1,2,3,*] He-Liang Huang,[1,2,3,*] Yiming Zhang,[1,2,3] Dachao Wu,[1,2,3] Huijie Guan,[1,2,3] Qingling Zhu,[1,2,3] Zuolin Wei,[1,2,3] Tan He,[1,2,3] Sirui Cao,[1,2,3] Fusheng Chen,[1,2,3] Tung-Hsun Chung,[1,2,3] Hui Deng,[1,2,3] Daojin Fan,[1,2,3] Ming Gong,[1,2,3] Cheng Guo,[1,2,3] Shaojun Guo,[1,2,3] Lianchen Han,[1,2,3] Na Li,[1,2,3] Shaowei Li,[1,2,3] Yuan Li,[1,2,3] Futian Liang,[1,2,3] Jin Lin,[1,2,3] Haoran Qian,[1,2,3] Hao Rong,[1,2,3] Hong Su,[1,2,3] Lihua Sun,[1,2,3] Shiyu Wang,[1,2,3] Yulin Wu,[1,2,3] Yu Xu,[1,2,3] Chong Ying,[1,2,3] Jiale Yu,[1,2,3] Chen Zha,[1,2,3] Kaili Zhang,[1,2,3] Yong-Heng Huo,[1,2,3] Chao-Yang Lu,[1,2,3] Cheng-Zhi Peng,[1,2,3] Xiaobo Zhu,[1,2,3] and Jian-Wei Pan[1,2,3]

[1]*Department of Modern Physics, University of Science and Technology of China, Hefei 230026, China*
[2]*Shanghai Branch, CAS Center for Excellence in Quantum Information and Quantum Physics, University of Science and Technology of China, Shanghai 201315, China*
[3]*Shanghai Research Center for Quantum Sciences, Shanghai 201315, China*

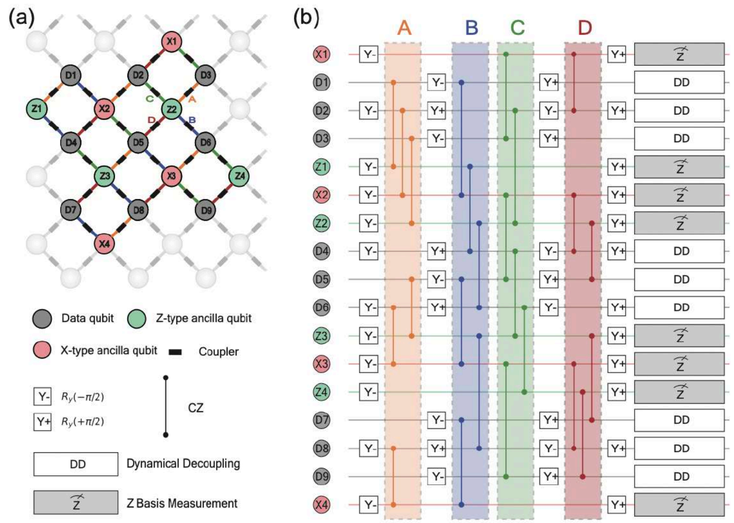

FIG. 1. **Layout and circuit implementation.** **(a)** Structure schematic of distance-three surface code. 17 qubits are choosen from *Zuchongzhi* 2.1 superconducting quantum processor, with 8 data qubits(gray dots), 4 Z-type ancilla qubits(green dots) and 4 X-type ancilla qubits(red dots). Each pair of qubits are connected with a coupler(black rectangle). Connecting lines are colored according

Ongoing experiments on error correction: Rydberg atoms

A quantum processor based on coherent transport of entangled atom arrays

Dolev Bluvstein[1], Harry Levine[1,†], Giulia Semeghini[1], Tout T. Wang[1], Sepehr Ebadi[1], Marcin Kalinowski[1], Alexander Keesling[1,2], Nishad Maskara[1], Hannes Pichler[3,4], Markus Greiner[1], Vladan Vuletić[5], and Mikhail D. Lukin[1]

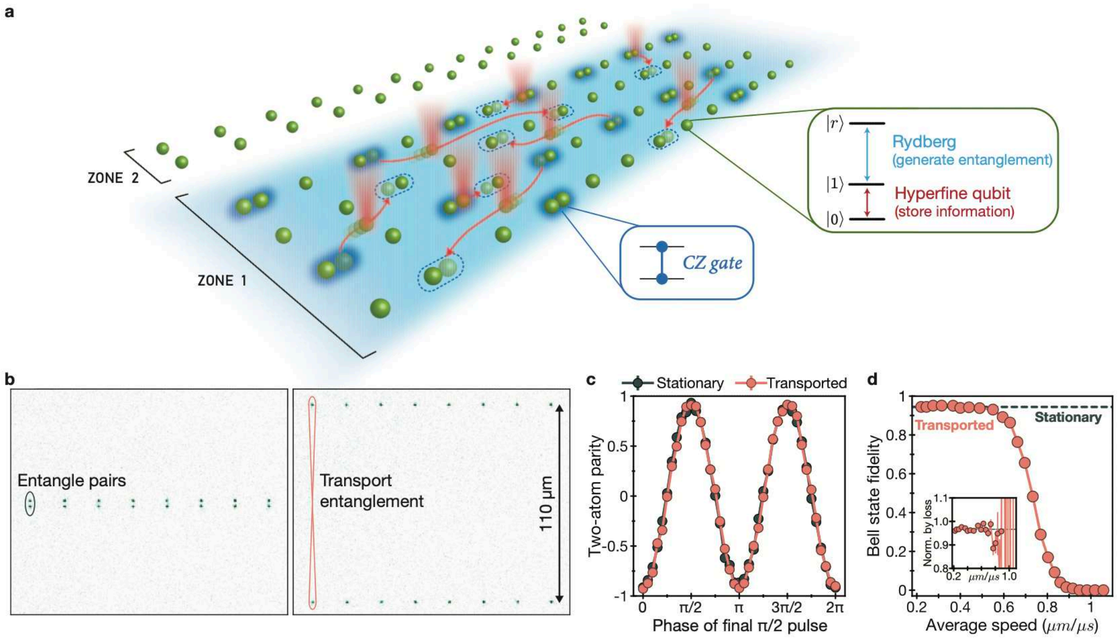

FIG. 1. **Quantum information architecture enabled by coherent transport of neutral atoms. a,** In our approach, qubits are transported to perform entangling gates with distant qubits, enabling programmable and nonlocal connectivity. Atom shuttling is performed using optical tweezers, with high parallelism in two dimensions and between multiple zones allowing selective manipulations. Inset shows the atomic levels used: the $|0\rangle$, $|1\rangle$ qubit states refer to the $m_F = 0$ clock states of ^{87}Rb, and $|r\rangle$ is a Rydberg state used for generating entanglement between qubits (Extended Data Fig. 1b). **b,** Atom images illustrating coherent transport of entangled qubits. Using a sequence of single-qubit and two-qubit gates, atom pairs are each prepared in the $|\Phi^+\rangle$ Bell state (Methods), and are then separated by 110 μm over a span of 300 μs. **c,** Parity oscillations indicate that movement does not observably affect entanglement or coherence. For both the moving and stationary measurements, qubit coherence is preserved using an XY8 dynamical decoupling sequence for 300 μs (Methods). **d,** Measured Bell state fidelity as a function of separation speed over the 110 μm, showing that fidelity is unaffected for a move slower than 200 μs (average separation speed of 0.55 μm/μs). Inset: normalizing by atom loss during the move results in constant fidelity, indicating that atom loss is the dominant error mechanism (see Methods for details).

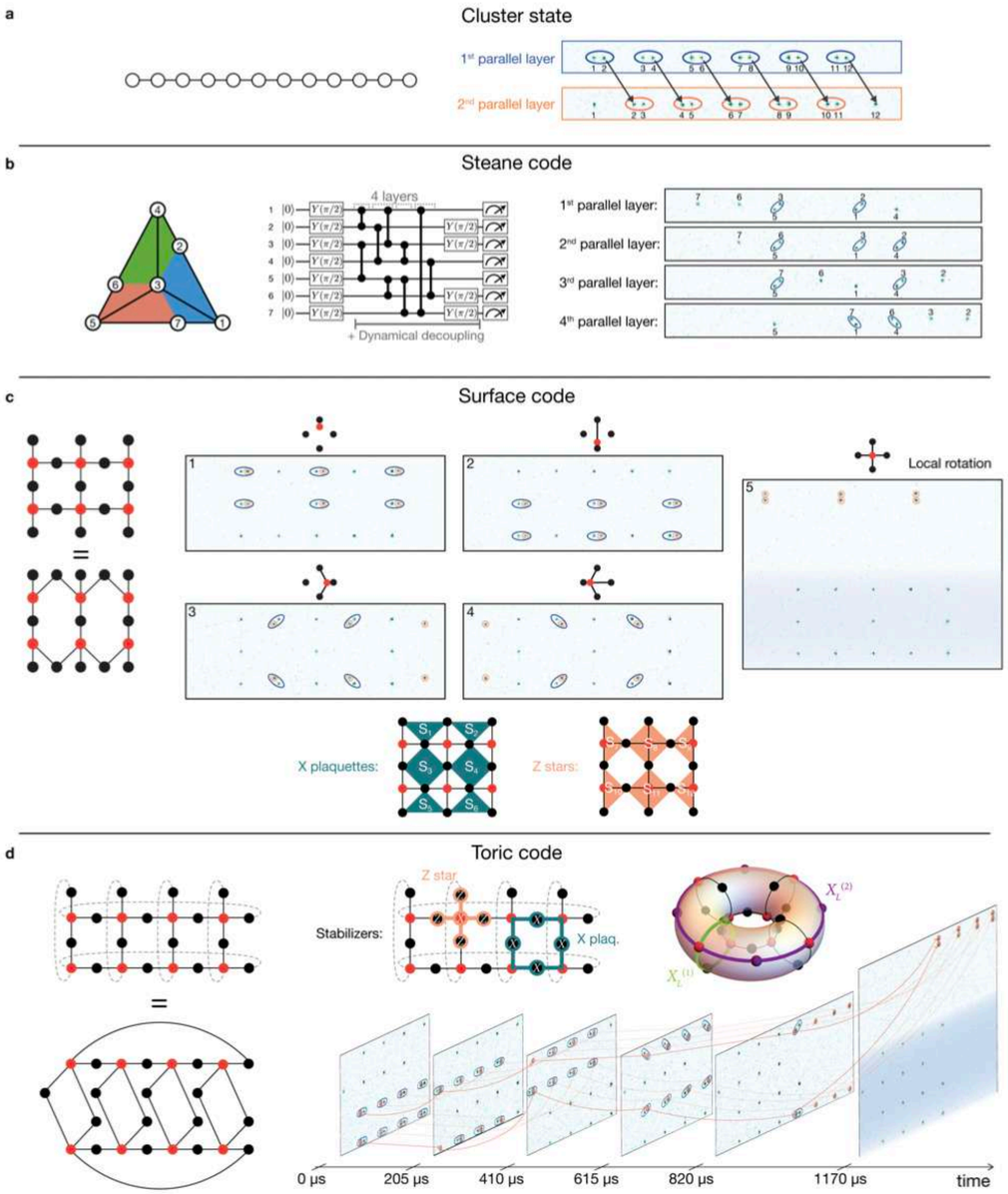

Ongoing experiments on error correction: Ions

Entangling logical qubits with lattice surgery

https://doi.org/10.1038/s41586-020-03079-6
Received: 1 July 2020
Accepted: 20 October 2020

Alexander Erhard[1,8], Hendrik Poulsen Nautrup[2,8], Michael Meth[1], Lukas Postler[1], Roman Stricker[1], Martin Stadler[3], Vlad Negnevitsky[3], Martin Ringbauer[1], Philipp Schindler[1], Hans J. Briegel[2,4], Rainer Blatt[1,5], Nicolai Friis[2,6]✉ & Thomas Monz[1,7]✉

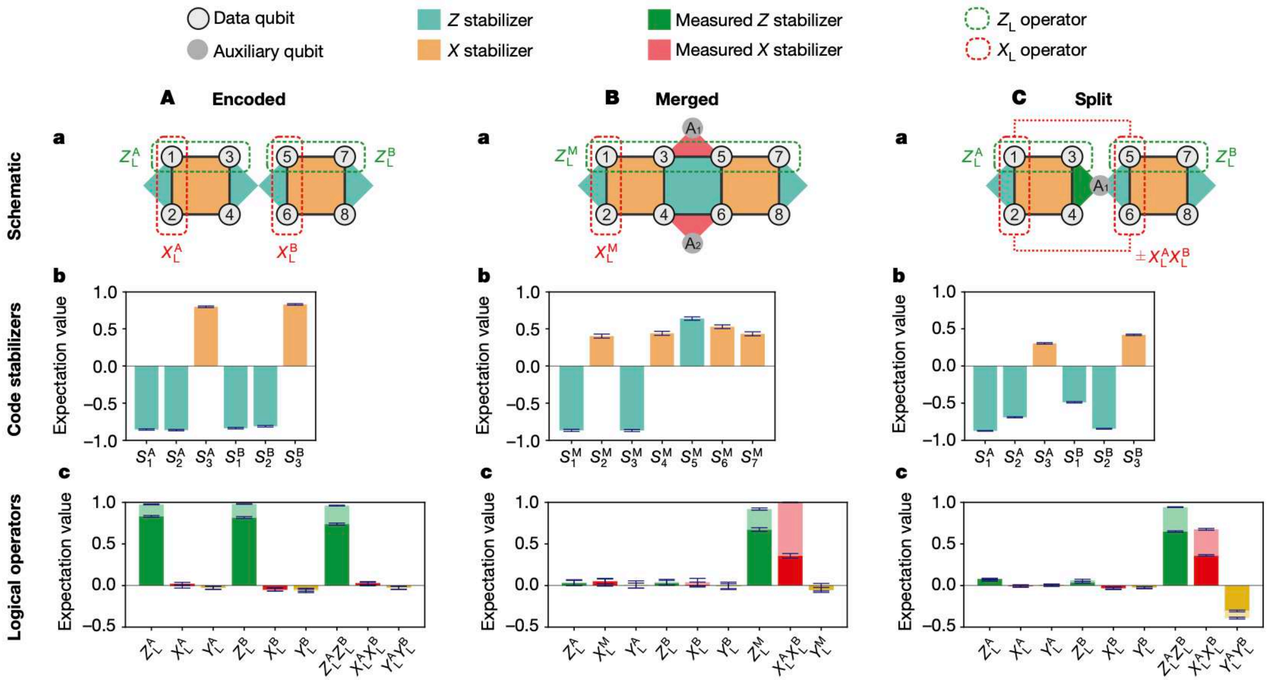

Fault-tolerant control of an error-corrected qubit

https://doi.org/10.1038/s41586-021-03928-y
Received: 23 September 2020

Laird Egan[1,2,10]✉, Dripto M. Debroy[4,11], Crystal Noel[1,2], Andrew Risinger[1,2,3], Daiwei Zhu[1,2,3], Debopriyo Biswas[1,2], Michael Newman[5,11], Muyuan Li[6,7], Kenneth R. Brown[4,5,6,7,8], Marko Cetina[1,2] & Christopher Monroe[1,2,3,4,5,9]

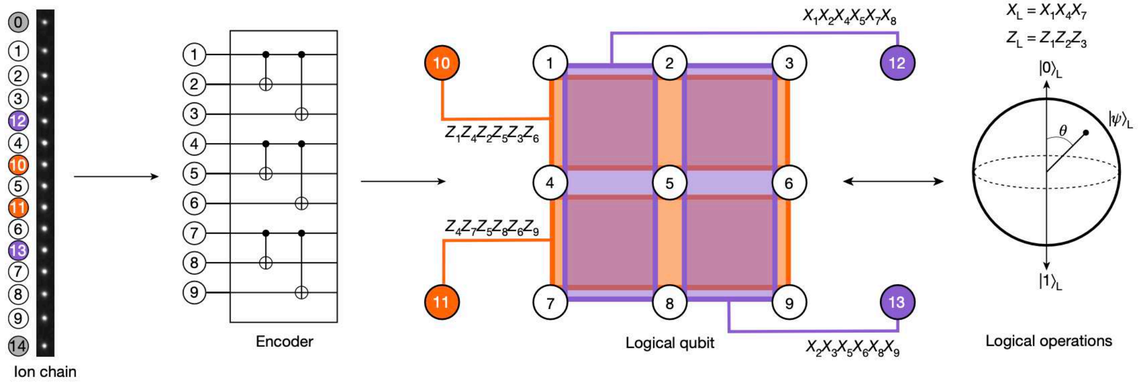

Fig. 1 | The Bacon–Shor subsystem code implemented on a 15-ion chain. Bacon–Shor is a [[9,1,3]] subsystem code that encodes nine data qubits into one logical qubit. Four weight-six stabilizers are mapped to ancillary qubits 10, 11, 12 and 13, for measuring errors in the X and Z basis. We demonstrate encoding of the logical qubit, with subsequent logical gate operations or error syndrome extraction.

Semiconductor qubits below the error threshold

Fast universal quantum gate above the fault-tolerance threshold in silicon

https://doi.org/10.1038/s41586-021-04182-y
Received: 4 August 2021
Accepted: 26 October 2021

Akito Noiri[1]✉, Kenta Takeda[1], Takashi Nakajima[1], Takashi Kobayashi[2], Amir Sammak[3,4], Giordano Scappucci[3,5] & Seigo Tarucha[1,2]✉

2-qubit gate fidelity of 99.5

Precision tomography of a three-qubit donor quantum processor in silicon

https://doi.org/10.1038/s41586-021-04292-7
Received: 29 June 2021
Accepted: 29 November 2021
Published online: 19 January 2022

Mateusz T. Mądzik[1,9,12], Serwan Asaad[1,10,12], Akram Youssry[2,3], Benjamin Joecker[1], Kenneth M. Rudinger[4], Erik Nielsen[4], Kevin C. Young[5], Timothy J. Proctor[5], Andrew D. Baczewski[6], Arne Laucht[1,2], Vivien Schmitt[1,11], Fay E. Hudson[1], Kohei M. Itoh[7], Alexander M. Jakob[8], Brett C. Johnson[8], David N. Jamieson[8], Andrew S. Dzurak[1], Christopher Ferrie[2], Robin Blume-Kohout[4] & Andrea Morello[1]✉

2-qubit average gate fidelity of 99.37(11)% and two-qubit preparation/measurement fidelities of 98.95(4)%

Quantum logic with spin qubits crossing the surface code threshold

https://doi.org/10.1038/s41586-021-04273-w
Received: 1 July 2021

Xiao Xue[1,2], Maximilian Russ[1,2], Nodar Samkharadze[1,3], Brennan Undseth[1,2], Amir Sammak[1,3], Giordano Scappucci[1,2] & Lieven M. K. Vandersypen[1,2]✉

1-qubit and 2-qubit gate fidelities, all of which are above 99.5%, extracted from gate-set tomography

Towards practical applications: Quantum annealing (for optimization and machine learning) and quantum chemistry

A.S. Boev, et. al. Genome assembly using quantum and quantum-inspired annealing, Scientific Reports 11, 13183 (2021); arXiv:2004.06719;

A. Gircha, et. al., Training a discrete variational autoencoder for generative chemistry and drug design on a quantum annealer, arXiv:2108.11644.

M. Sapova and A.K. Fedorov,
Variational quantum eigensolver techniques for simulating carbon monoxide oxidation, arXiv:2108.11167

From universal quantum computers to special-purpose quantum devices

D-Wave quantum annealer for QUBO problems

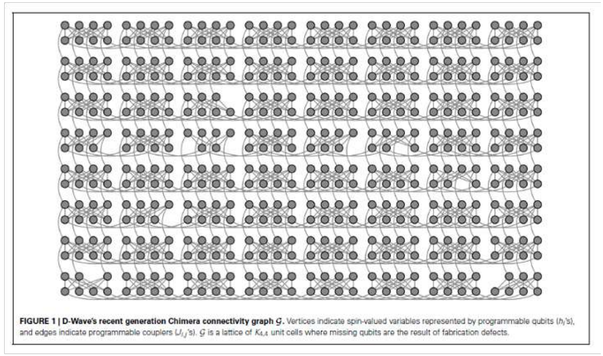

FIGURE 1 | D-Wave's recent generation Chimera connectivity graph $\mathcal{G}$. Vertices indicate spin-valued variables represented by programmable qubits (h_i's), and edges indicate programmable couplers ($J_{i,j}$'s). $\mathcal{G}$ is a lattice of $K_{4,4}$ unit cells where missing qubits are the result of fabrication defects.

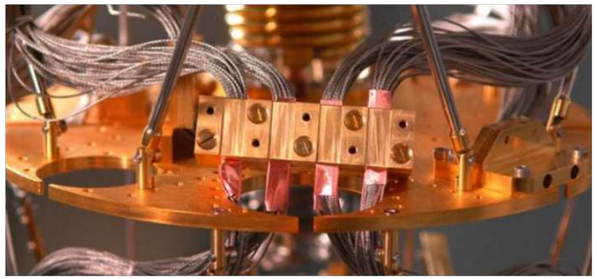

Lack of connectivity, coherence, violating adiabatic evolution, access for experiments

Rydberg programmable quantum simulators for MIS problems

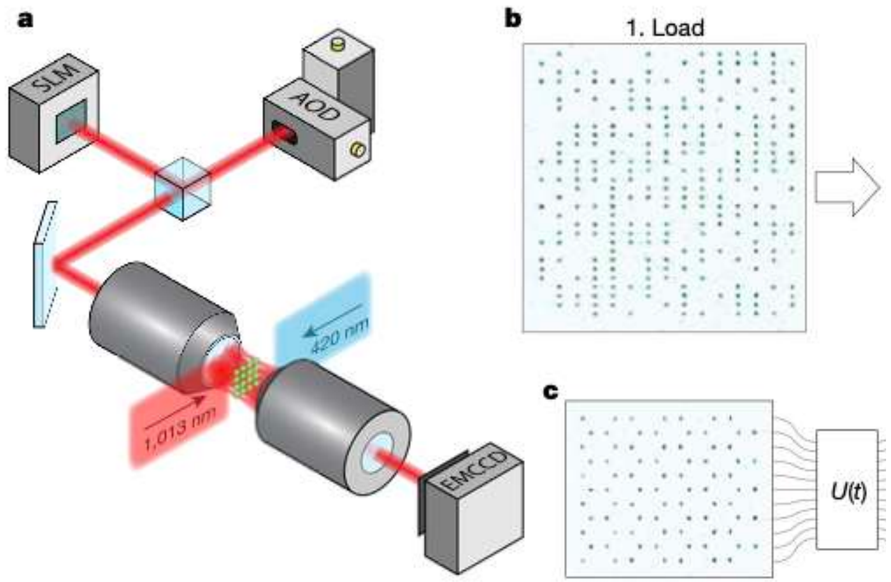

Potentially better coherence, connectivity, not yet widely available

From universal quantum computers to special-purpose quantum devices

It consists in finding the bit string ($\sigma_i = \pm 1$) that minimize the objective function, $H = \sum_i R_i \sigma_i - \frac{1}{2} \sum_{i,j} J_{ij} \sigma_i \sigma_j$, where R_i is the "bias vector" and $J_{ij} = J_{ji}$ is a given "coupling matrix". This objective function emerges in solid state physics under the name of Ising models, hence QUBO is sometimes referred to as Ising problem.

Many potential applications:

- designing metamaterials,
- quantum chemistry (not scalable),
- protein folding (not scalable),
- financial portfolio optimization,
- forecasting financial crashes,
- scheduling
- …

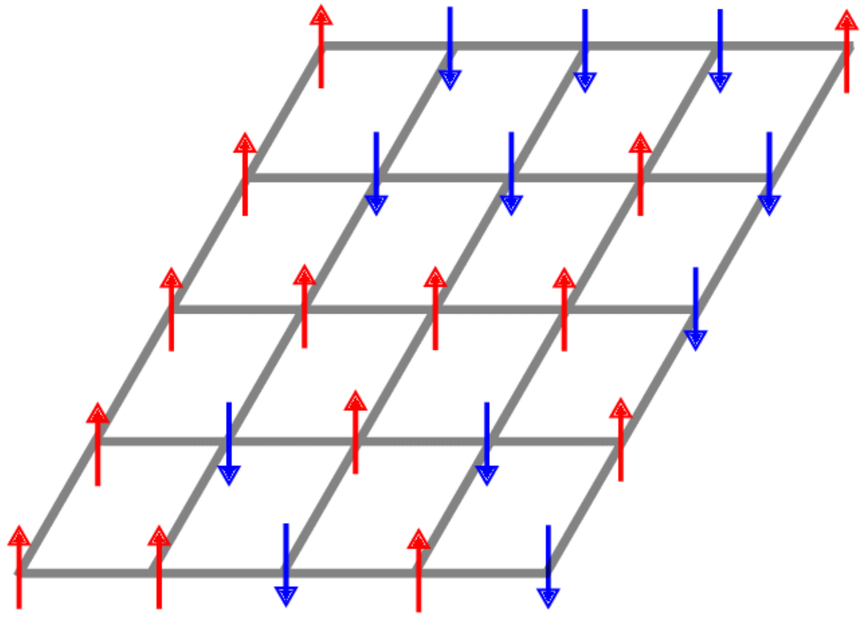

Quantum annealing for a genome assembly problem

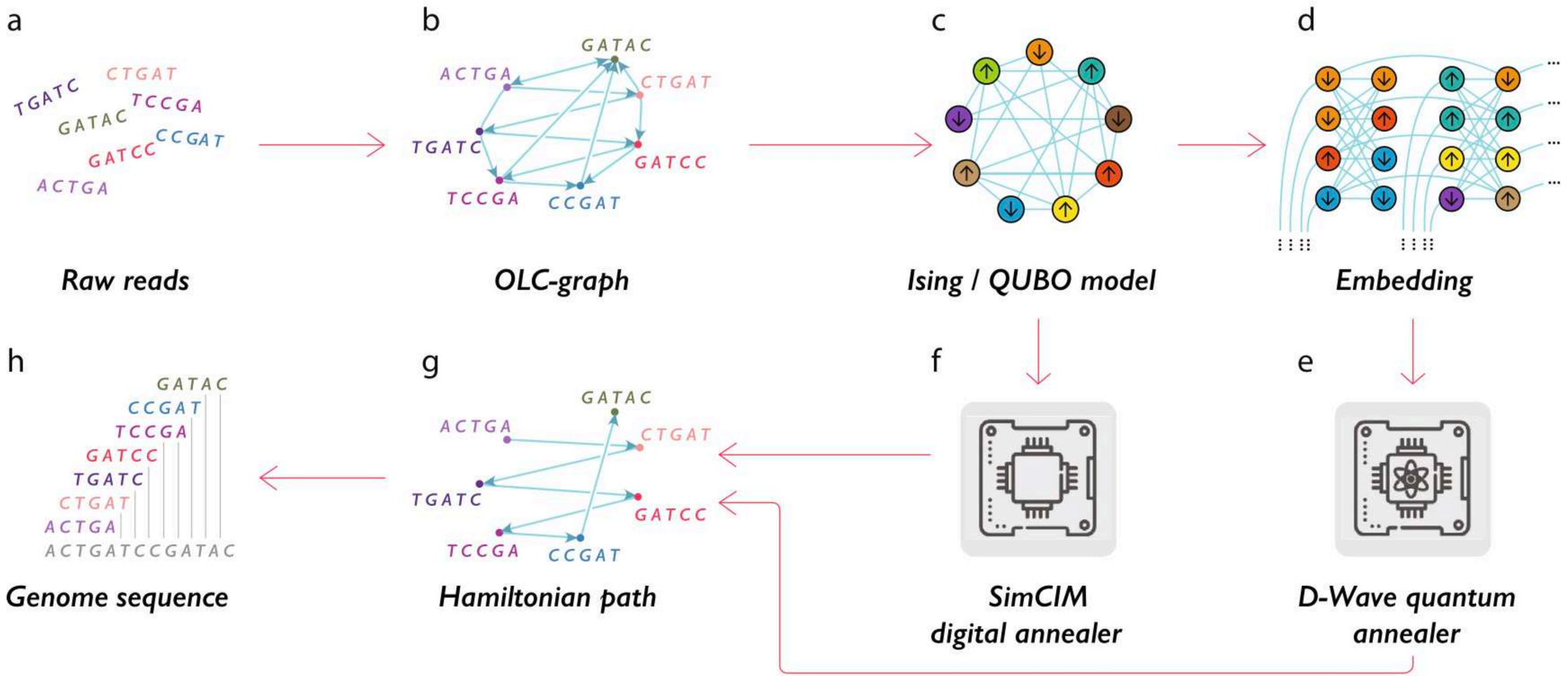

Figure 1. Solving the *de novo* genome assembly problem using quantum annealers and quantum-inspired (digital) annealing algorithms: (**a**) raw reads; (**b**) raw reads are transformed to the overlap-layout-consensus (OLC) graph; (**c**) finding the Hamiltonian path for the OLC graph is reduced to the QUBO problem; (**d**) the QUBO problem should be embedded to the architecture of the quantum annealer (D-Wave): for this purpose each logical variable of the the QUBO problem is assigned with several qubits of the quantum annealer; (**e**) and (**f**) the Ising problem in QUBO form can be solved using quantum annealers (D-Wave) and quantum-inspired algorithms (SimCIM), correspondingly; (**g**) the output is the Hamiltonian path; (**h**) the genome sequence is obtained as the solution.

Quantum annealing for a genome assembly problem

		Mean, μs	Min, μs	Max, μs	90%
Quantum annealer	CPU	8483	8314	8619	8579
	QPU	535	369	672	600
Quantum-inspired annealer (SimCIM)		262	9.9	7212	1061

Table 1. Genome assembly time for ϕX 174 bacteriophage for 1000 instances. For the data based on experiments with quantum annealers we highlight required classical processor unit (CPU) time and quantum processor unit (QPU) time.

Experiments characteristics:

- annealing time = 20 microseconds;
- annealing runs = 10^3;
- standard configurations of the processor.

Quantum annealing for a genome assembly problem

$$\mathrm{TTS} = t_a R_{99},$$

Sequence length	Graph size	Qubo size	Physical qubits
5	3	9	36
6	4	16	80
7	5	25	200
8	6	36	360
9	7	49	686
10	8	64	1088

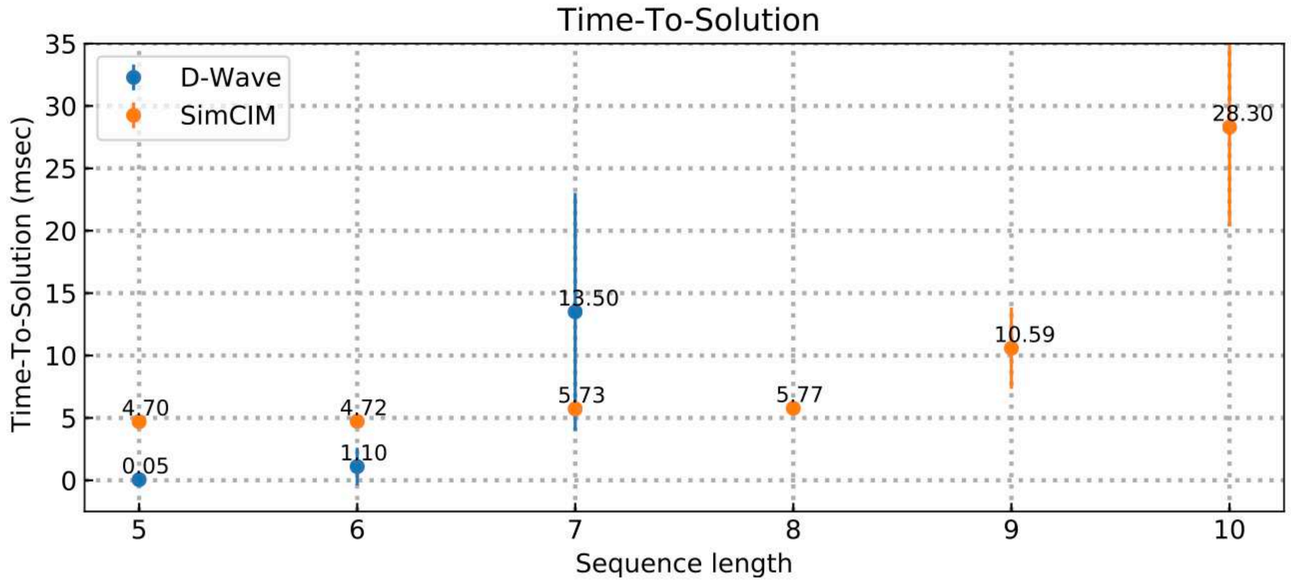

Figure 2. Comparison of the performance of quantum and quantum-inspired methods for *de novo* genome assembly based on synthetic data (10 problems were generated for every sequence length): we compare TTS for quantum device D-Wave and quantum-inspired optimization algorithm SimCIM.

Competitive behaviour for small-size data, but growing overhead in the size of the problem number of physical qubits and other limitations… need better hardware (coherence and connectivity)

Quantum annealing for generative chemistry

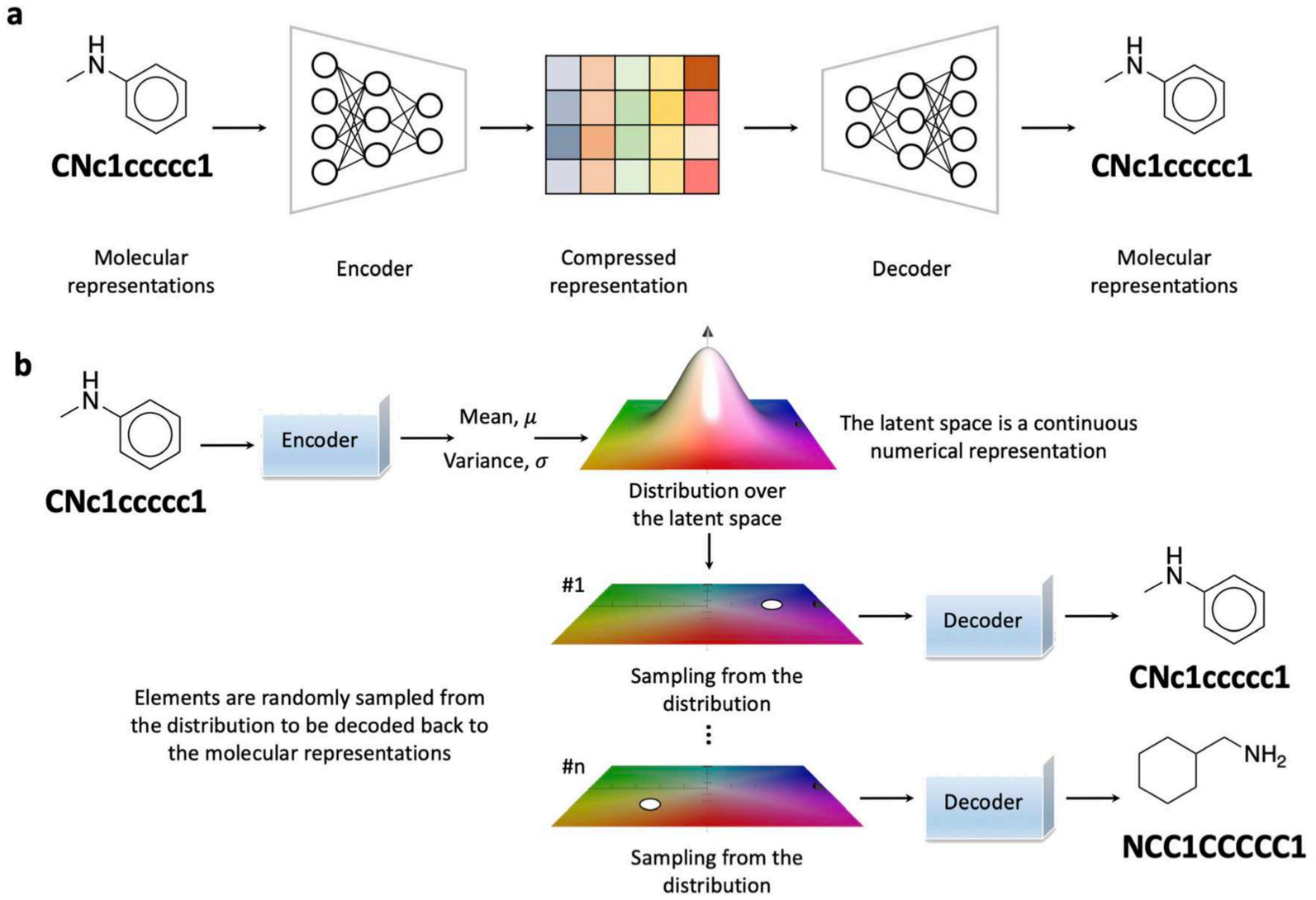

Fig. 3 The autoencoder and the variational autoencoder. **a** An autoencoder encodes input molecules into compressed representations and decodes them back. **b** A variational autoencoder maps the molecules into the parameters of a statistical distribution as the latent space is a continuous numerical representation

Quantum annealing for training

Existing special-purpose quantum devices can be used for this purpose. Dumoulin et al. [325] and Benedetti et al. [326] pointed out that quantum annealers that have strong interaction with the environment freeze out the dynamics of a spin system before the termination of the annealing process. As a result, such annealers sample from a thermal distribution with some finite temperature. The proposed method was experimentally implemented using the D-Wave 2X quantum annealer [97, 326] for the training of a Boltzmann machine. However, shortcomings of existing quantum annealers (see Box 8) limited the study to low-dimensional datasets.

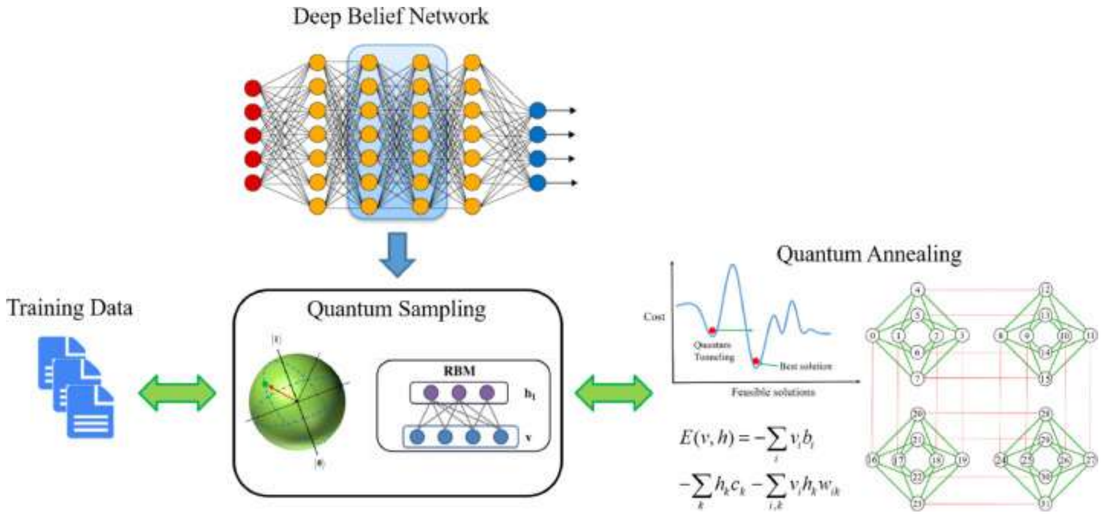

Training Restricted Boltzmann Machines With a D-Wave Quantum Annealer

Vivek Dixit*[1,2], *Raja Selvarajan*[1,2], *Muhammad A. Alam*[3,4], *Travis S. Humble*[5] and *Sabre Kais*[1,2,4]

[1]Department of Chemistry, Purdue University, West Lafayette, IN, United States, [2]Department of Physics and Astronomy, Purdue University, West Lafayette, IN, United States, [3]Department of Electrical and Computer Engineering, Purdue University, West Lafayette, IN, United States, [4]Birck Nanotechnology Center, Purdue University, West Lafayette, IN, United States, [5]Quantum Computing Institute, Oak Ridge National Laboratory, Oak Ridge, TN, United States

Restricted Boltzmann Machine (RBM) is an energy-based, undirected graphical model. It is commonly used for unsupervised and supervised machine learning. Typically, RBM is trained using contrastive divergence (CD). However, training with CD is slow and does not estimate the exact gradient of the log-likelihood cost function. In this work, the model expectation of gradient learning for RBM has been calculated using a quantum annealer (D-Wave 2000Q), where obtaining samples is faster than Markov chain Monte Carlo (MCMC) used in CD. Training and classification results of RBM trained using quantum annealing are compared with the CD-based method. The performance of the two approaches is compared with respect to the classification accuracies, image reconstruction, and log-likelihood results. The classification accuracy results indicate comparable performances of the two methods. Image reconstruction and log-likelihood results show improved performance of the CD-based method. It is shown that the samples obtained from quantum annealer can be used to train an RBM on a 64-bit "bars and stripes" dataset with classification performance similar to an RBM trained with CD. Though training based on CD showed improved learning performance, training using a quantum annealer could be useful as it eliminates computationally expensive MCMC steps of CD.

Quantum annealing for generative chemistry

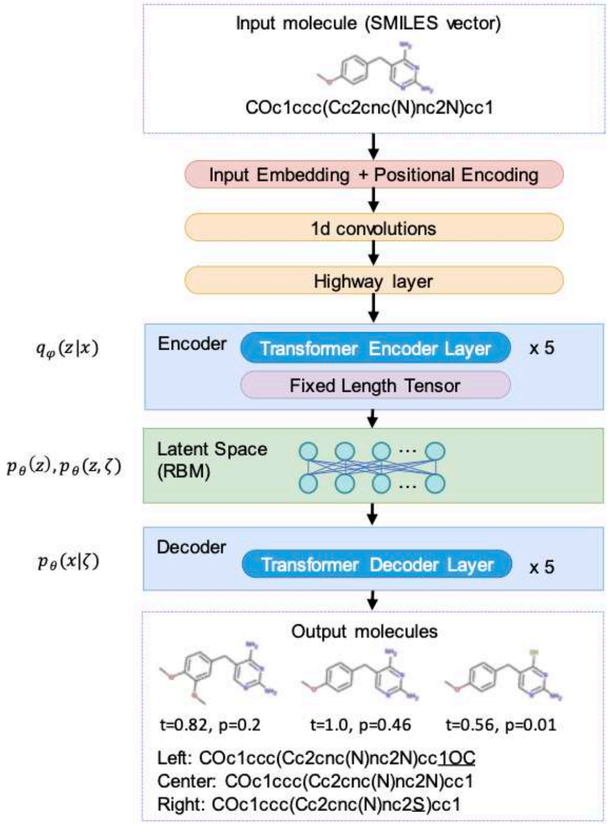

Figure 1. Scheme of the DVAE learning a joint probability distribution over the molecular structural features x and their latent variable-representations (discrete z and continuous ζ). Here, $q_\phi(z|x)$ and $p_\theta(x|\zeta)$ are the encoder and decoder distributions, respectively, whereas $p_\theta(z)$ is the prior distribution in the latent variable space and is approximated by RBM. We provide an example of reconstruction of a target molecule (diaveridine) using Gibbs-300 model saved after 300 epochs of training (here t is the Tanimoto similarity between the initial molecule and its reconstruction, $t = 1.0$ corresponds to perfect reconstruction, p is the output probability).

The model learns useful representations of chemical structures from ChEMBL, which is the manually curated database of biologically active molecules with drug-like properties

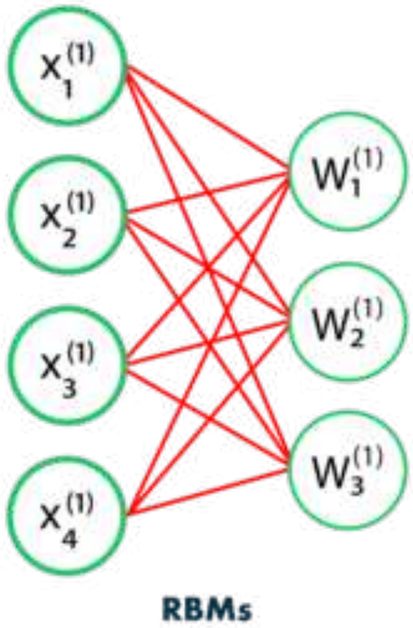

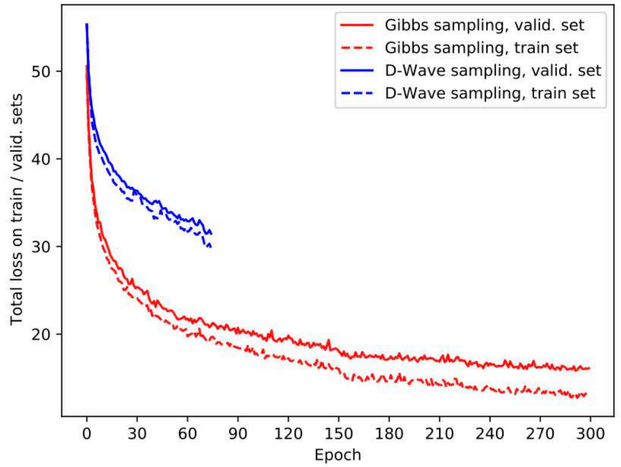

Figure 2. Learning curves of DVAE trained with classical Gibbs sampleing (red) and samples from D-Wave annealer (blue). Training on D-Wave suspended before reaching convergence due to resource limitation.

The two layers of RBM contain 128 units each since an RBM of precisely this size could be sampled on readily available quantum annealers.

Quantum annealing for generative chemistry

	Train set	D-Wave sampl. (75 epochs)	Gibbs sampl. (75 epochs)	Gibbs sampl. (300 epochs)
MW	409.99	374.16	397.81	416.14
LogP	3.41	3.68	3.64	3.61
QED	0.54	0.54	0.54	0.52
SAS	2.96	3.12	3.04	3.13
Validity	1.0	0.54	0.55	0.69

Table I. The parameters of distributions of basic physical and medicinal chemistry properties of the molecules produced by the generative models discussed in this work. The entries in the table are mean values computed with the help of RDKit library [29] to obtain the molecular weight (MW), LogP, QED, and the synthetic accessibility score (SAS) [28].

We kept track of molecular weight (MW), the water-octanol partition coefficient (logP), the synthetic accessibility, and drug-likeness (QED) scores; we generated 2331 novel chemical structures with medicinal chemistry and synthetic accessibility properties in the ranges typical for molecules from ChEMBL.

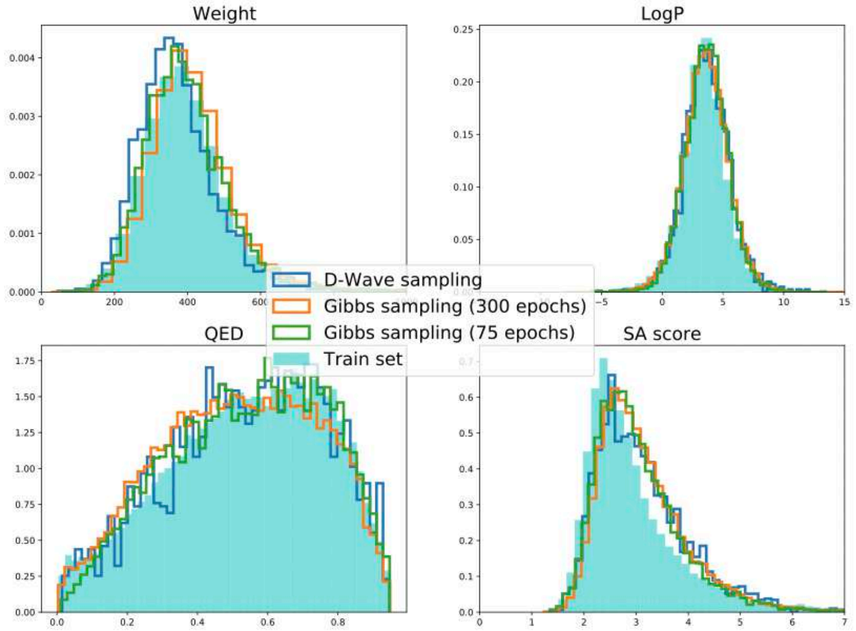

Figure 3. Distributions of basic physical and medicinal chemistry properties of the molecules produced by the proposed generative models discussed (same as in Table I).

Variational quantum algorithms

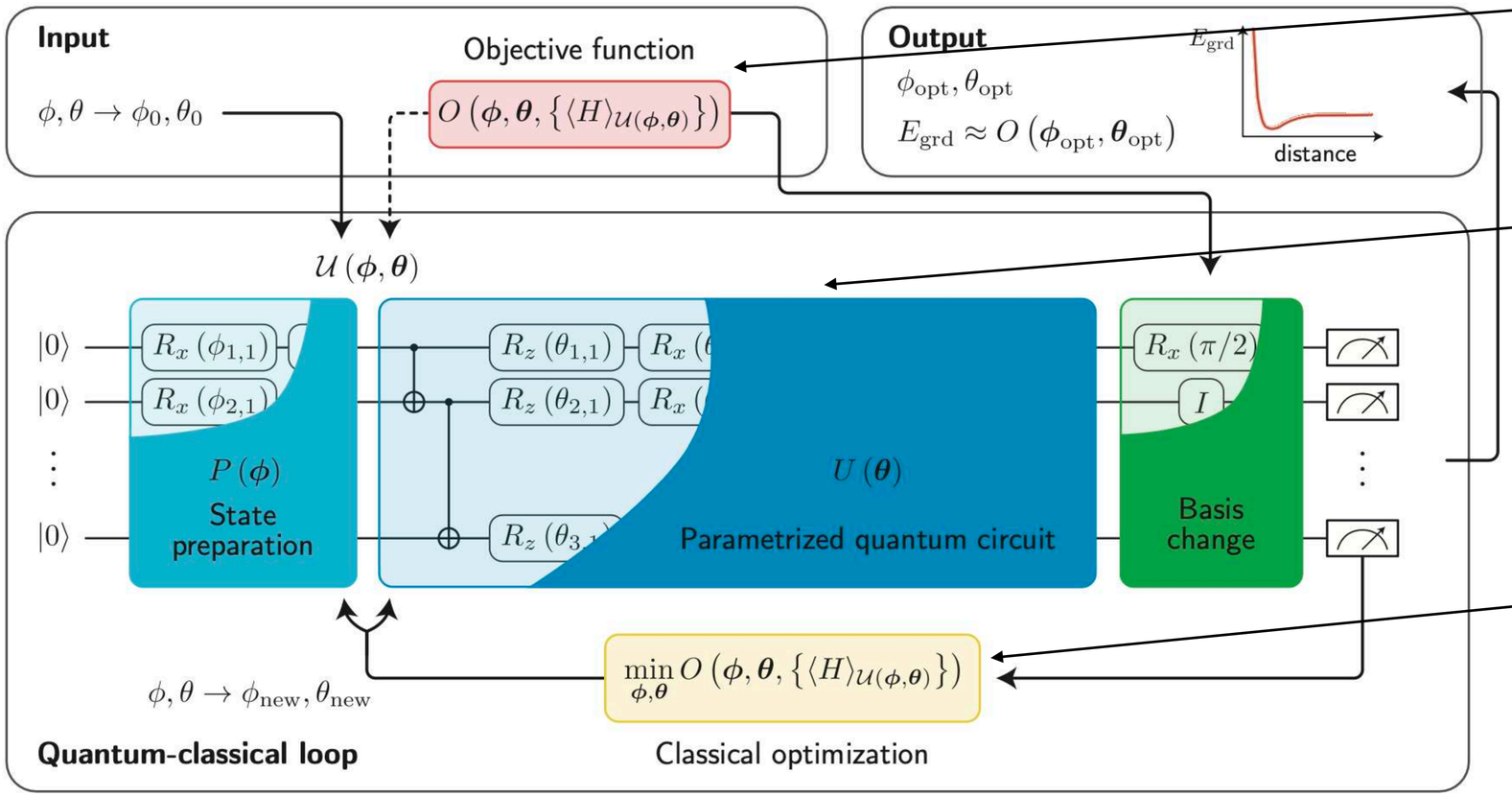

Problem to be solved

Design a parametrized quantum circuit

Classical calculations and feedback

Figure 2 Diagrammatic representation of a Variational Quantum Algorithm (VQA). A VQA workflow can be divided into four main components: *i)* the objective function O that encodes the problem to be solved; *ii)* the parameterized quantum circuit (PQC), in which its parameters $\boldsymbol{\theta}$ are tuned to minimize the objective; *iii)* the measurement scheme, which performs the basis changes and measurements needed to compute expectation values $\langle H \rangle$ that are used to evaluate the objective; and *iv)* the classical optimizer that minimizes the objective and proposes a new set of variational parameters. The PQC can be defined heuristically, following hardware-inspired ansätze, or designed from the knowledge about the problem Hamiltonian H. It can also include a state preparation unitary $P(\boldsymbol{\phi})$ which situates the algorithm to start in a particular region of parameter space. Inputs of a VQA are the circuit ansatz $\mathcal{U}(\boldsymbol{\theta}, \boldsymbol{\phi})$ and the initial parameter values $\boldsymbol{\theta}_0, \boldsymbol{\phi}_0$. Outputs include optimized parameter values $\boldsymbol{\theta}_{\text{opt}}, \boldsymbol{\phi}_{\text{opt}}$ and the minimum of the objective.

Variational quantum algorithms: VQE

Variational Quantum Eigensolver (VQE) is a flagship hybrid quantum-classical algorithm for molecular simulations. An extended family of algorithms.

ADAPT-VQE. Early variational algorithms employed a fixed ansatz design, with its parameters tuned using some classical optimizer. The "Adaptive Derivative-Assembled Pseudo-Trotter ansatz Variational Quantum Eigensolver" (ADAPT-VQE) was introduced as a more scalable and efficient way to simultaneously design and optimize a parameterized ansatz (Grimsley *et al.*, 2019b). At each iteration, ADAPT-VQE constructs an ansatz by adding an operator corresponding to the largest gradient from a carefully designed operator pool. That is, given an operator $\hat{\tau}_i$ from the operator pool, the gradient of the energy with respect to the corresponding parameter θ_i is defined as

$$\partial_i E = \langle\psi| [H, \hat{\tau}_i] |\psi\rangle , \tag{49}$$

where $|\psi\rangle$ is the ansatz at the current iteration to be updated. After computing the gradient components and choosing the operator corresponding to the largest gradient, the gate operation implementing $\hat{\tau}_i$ is added to the ansatz with its parameter value initialized at 0. The ansatz is then optimized before growing another operator. The ADAPT-VQE algorithm terminates when the norm of the gradient vector falls below a defined threshold. In the case of fermionic ADAPT-VQE, the operator pool consists of fermionic operators that are transformed into quantum gate operations through e.g. the Jordan-Wigner mapping. A more "hardware-efficient" variant of the ADAPT-VQE algorithm is the qubit ADAPT-VQE, in which the pool consists of gate operators acting directly on qubits (Tang *et al.*, 2019). Both versions of ADAPT-VQEs were able to to generate optimized circuits with reduced depths and CNOT counts compared to previous ansatz construction and optimization methods.

Variational quantum algorithms: VQE

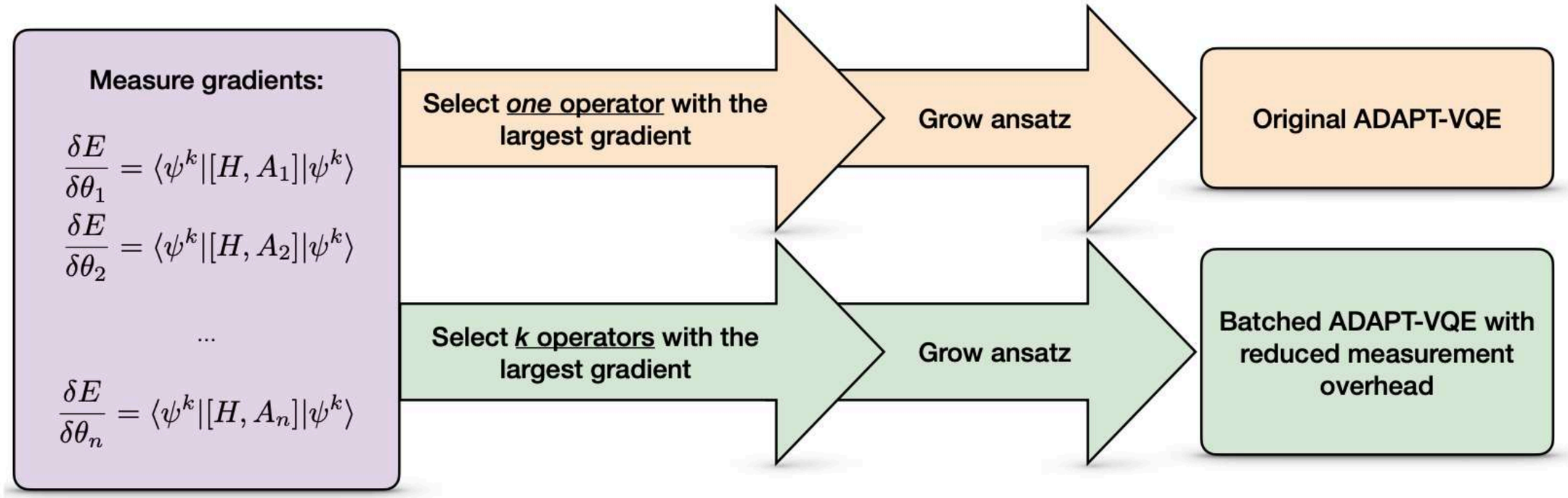

Figure 1. **Scheme of the ansatz growing procedure in original and batched ADAPT-VQE.** At each iteration, the original ADAPT-VQE adds a single operator with the largest gradient value. In our implementation of batched ADAPT-VQE, at each step of the ansatz growing procedure we add multiple operators with largest gradients; k is the number of gradients that differ from the largest one by less than r.

First results of VQE for O_2, CO, CO_2: 20-qubit emulator

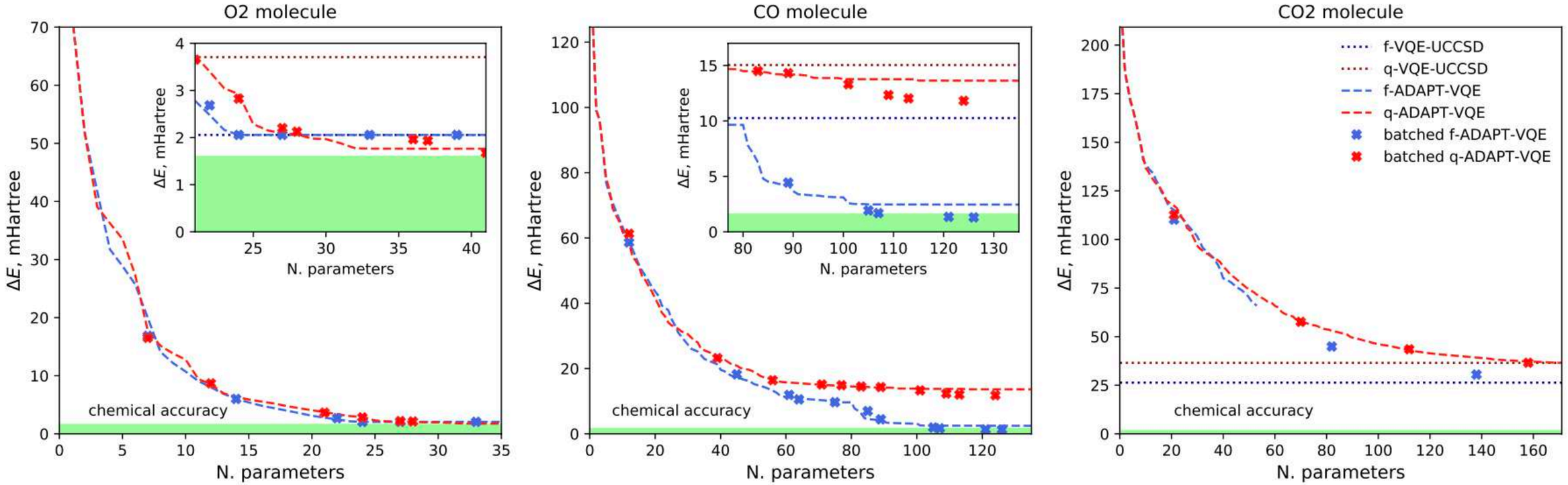

Figure 3. **Energy convergence for the considered implementations of ADAPT-VQE and VQE-UCCSD methods for O_2 (a), CO (b) and CO_2 (c) molecules.** We run batched ADAPT-VQE for all molecules beyond the simulation of original ADAPT-VQE. While for O_2 and CO molecules the original implementation converges, batched implementation continues to improve the energy. For CO_2, the original ADAPT-VQE takes infeasible amount of time, while batched version is much faster. We run limited iterations of the original ADAPT-VQE implementation to verify the similarity with batched ADAPT-VQE convergence.

Error correction codes: First steps

Error correction codes: First ideas and tests

- Wide class of codes (Special structure of stabilisers): repetition codes, Shor's code,…
- Circle-like connectivity (no all-to-all / ancilla-to-all)
- Low-noise two-qubit gates
- New efficient decoding system

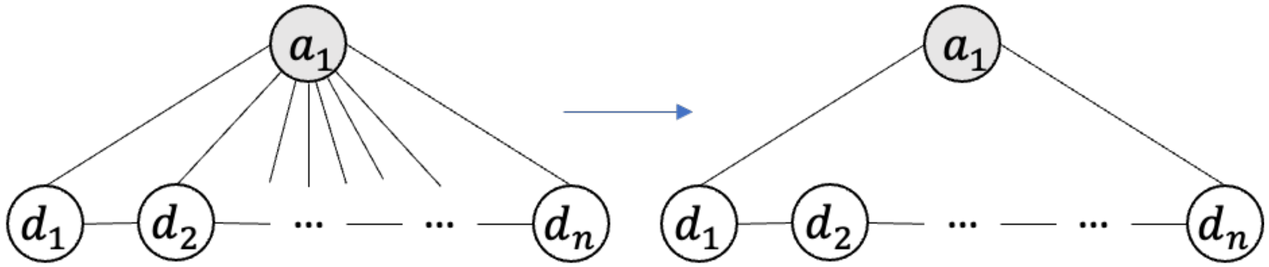

3-qubit code

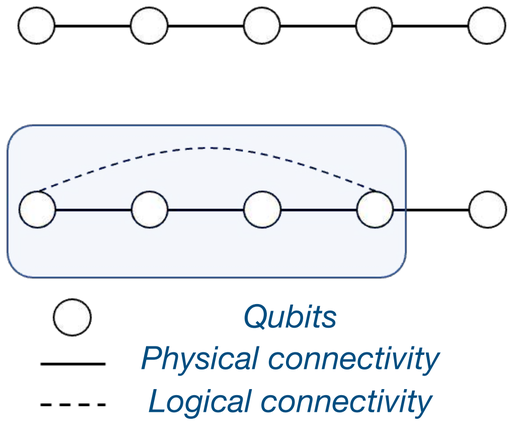

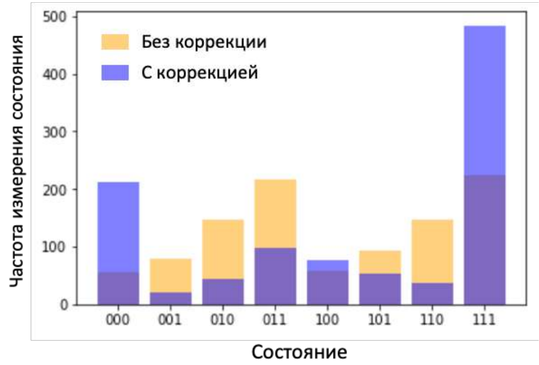

5-qubit code

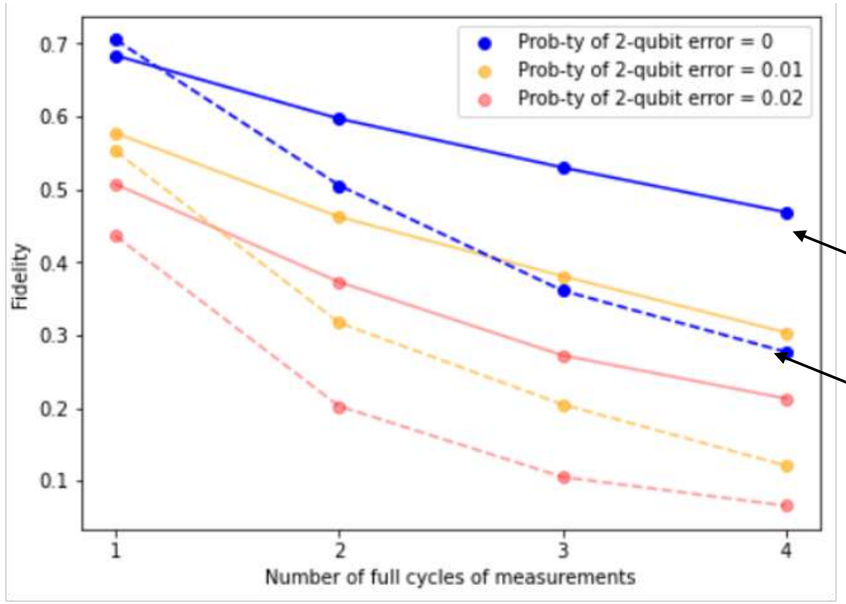

Correction

No correction

See also: I. A. Simakov, I. S. Besedin, and A. V. Ustinov, Simulation of the five-qubit quantum error correction code on superconducting qubits

Characterizing noisy devices

NISQ devices as open quantum systems

Challenge: analyze and predict dynamics of open quantum systems

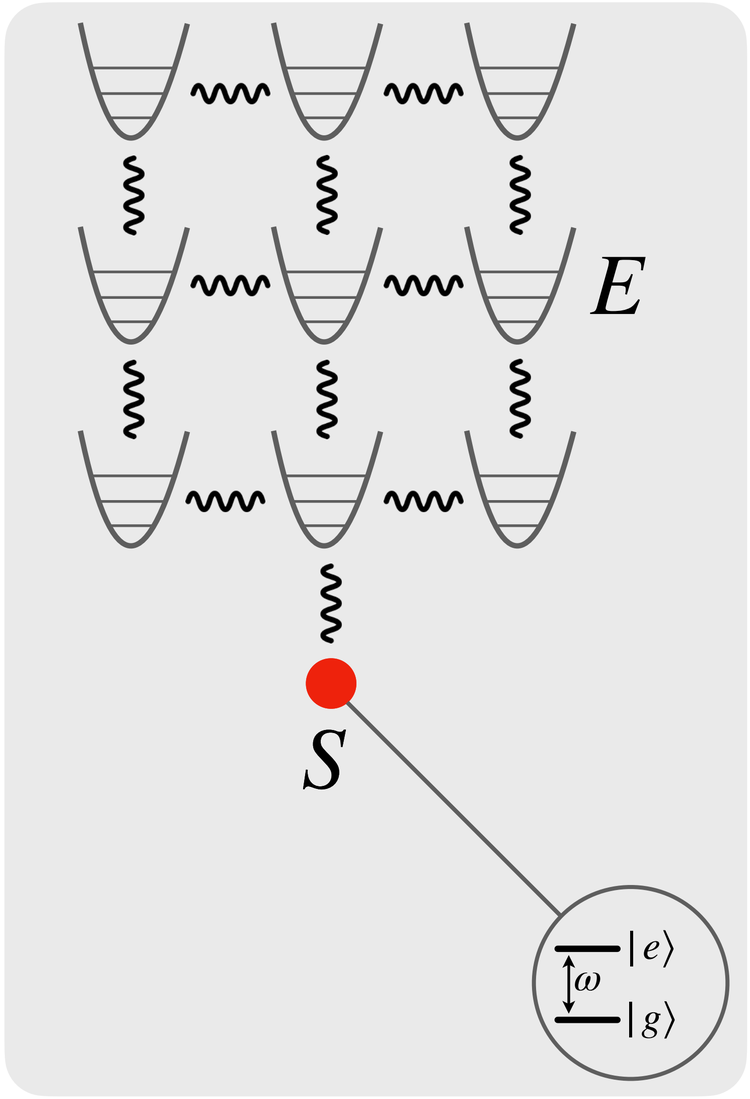

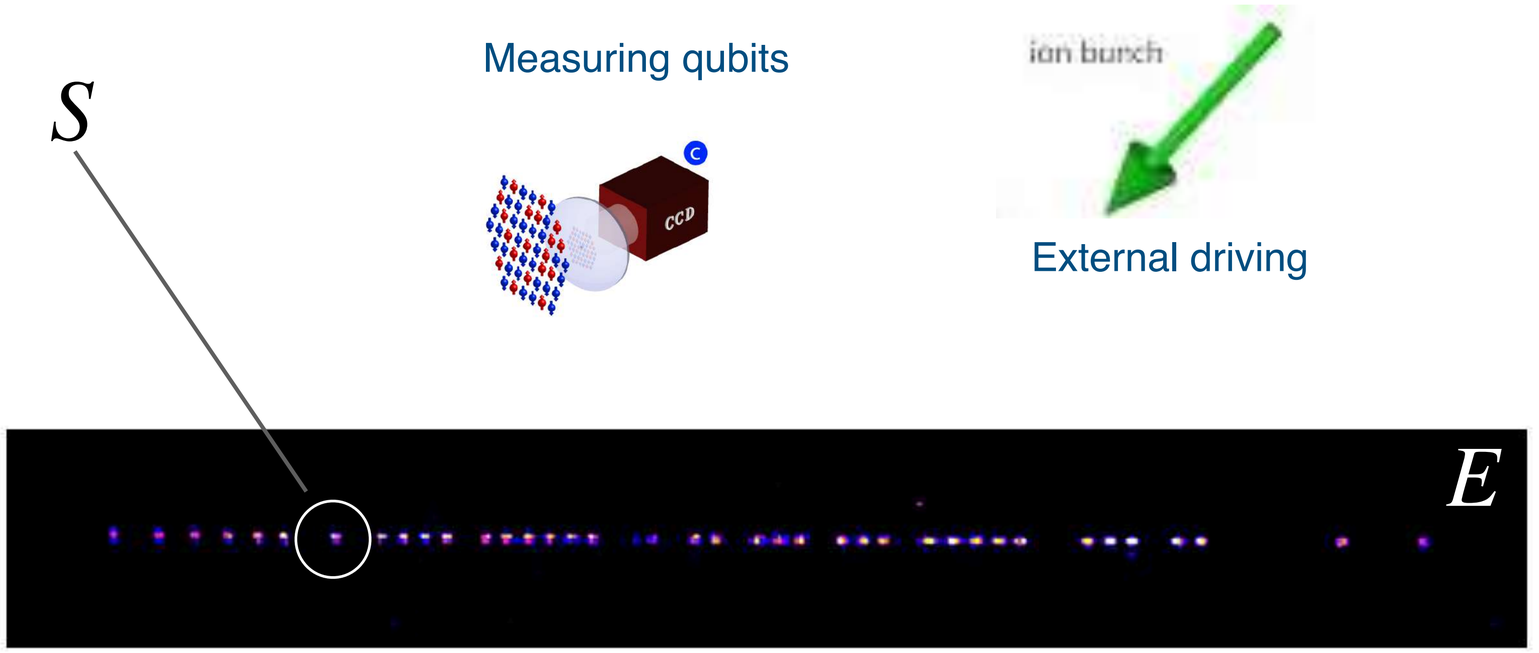

FIG. 2. A crystal of 38 laser-cooled $^{24}Mg^{+}$ ions loaded with the LED-loading method. Fluorescence from laser radiation at 280 nm is recorded by an EMCCD camera. Dark sites correspond to ions of other isotopes or elements.

I. Zalivako et. al., Appl. Phys. Lett. 115, 104102 (2019)

NISQ devices as open quantum systems: Learning

Goal is to analyze non-equilibrium dynamical effects of quantum physics. One of the problems is to make a prediction of the dynamics.

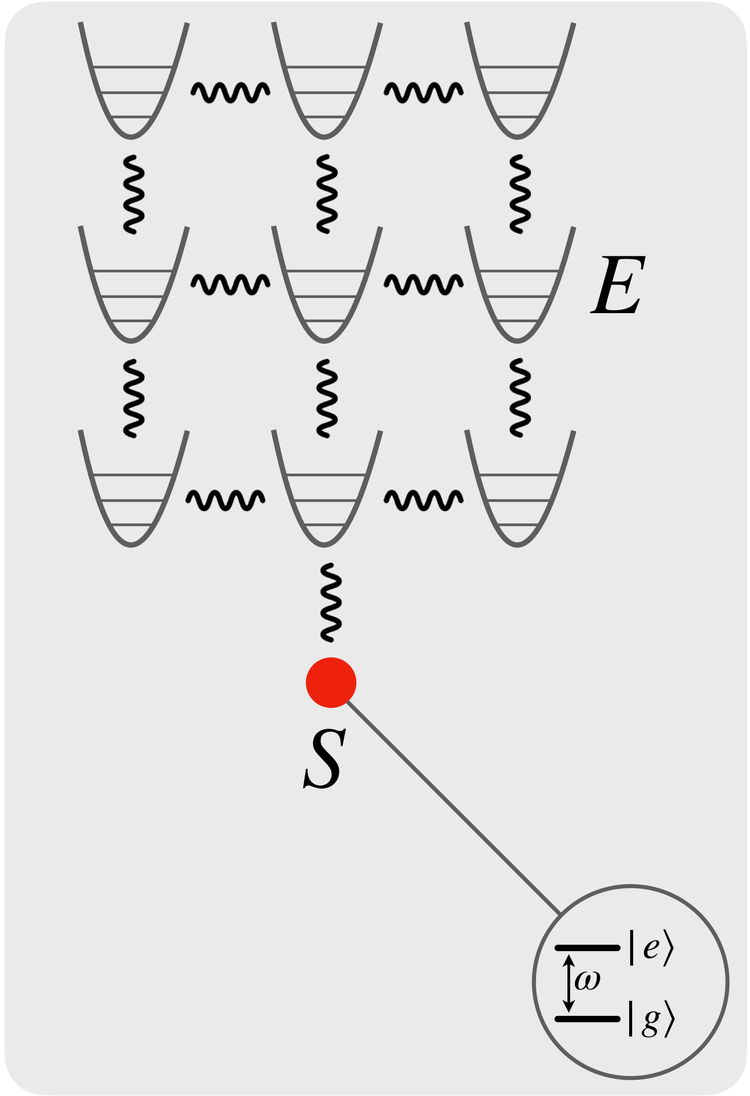

A possible solution: to use a data-driven approach (learning non-Markovian dynamics).

Advantages: can be based on experimentally observed data.

Disadvantages: “black-box” approaches (no physical insights about the system), scalability, convergence, and model selection.

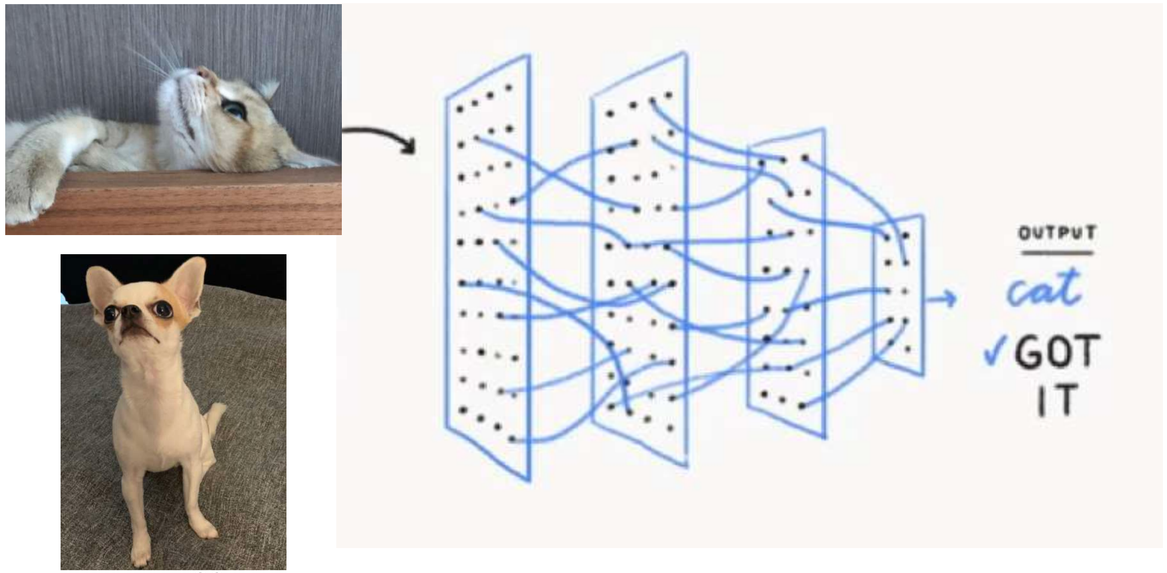

Probing non-Markovian dynamics: General scheme

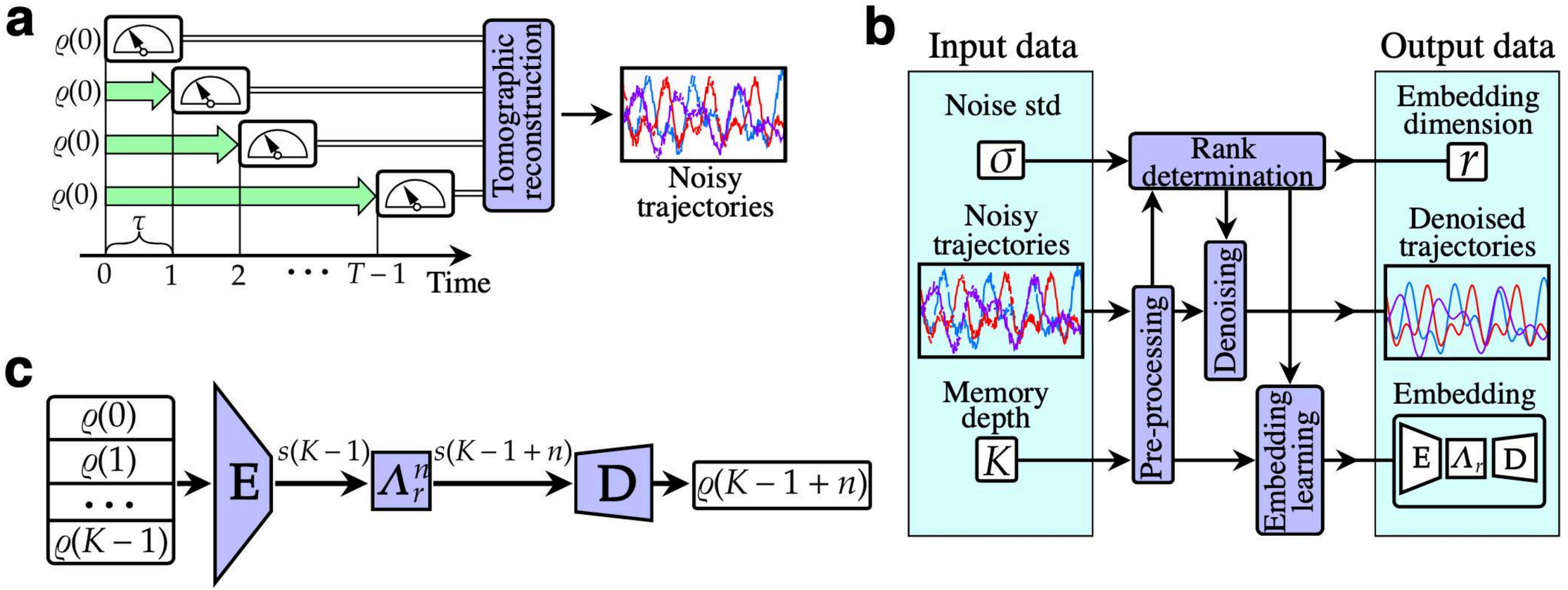

a) Extraction of quantum trajectories via quantum tomography of system states at discrete time moments. b) Main building blocks of the input data processing and connections between blocks. c) Dynamics prediction based on the reconstructed Markovian embedding.

Dynamics prediction and denoising for various models

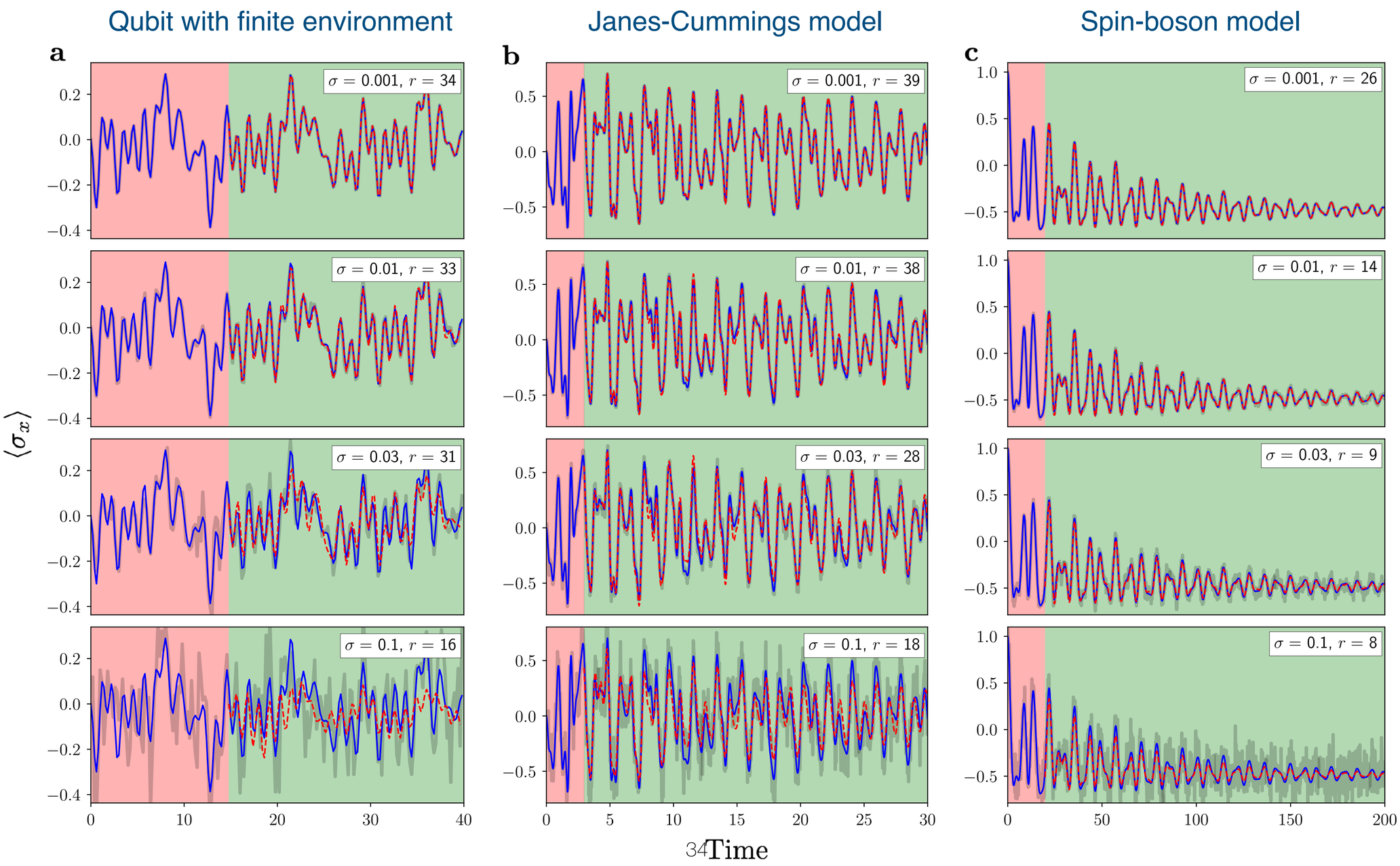

Characterizing quantum channels (processes)

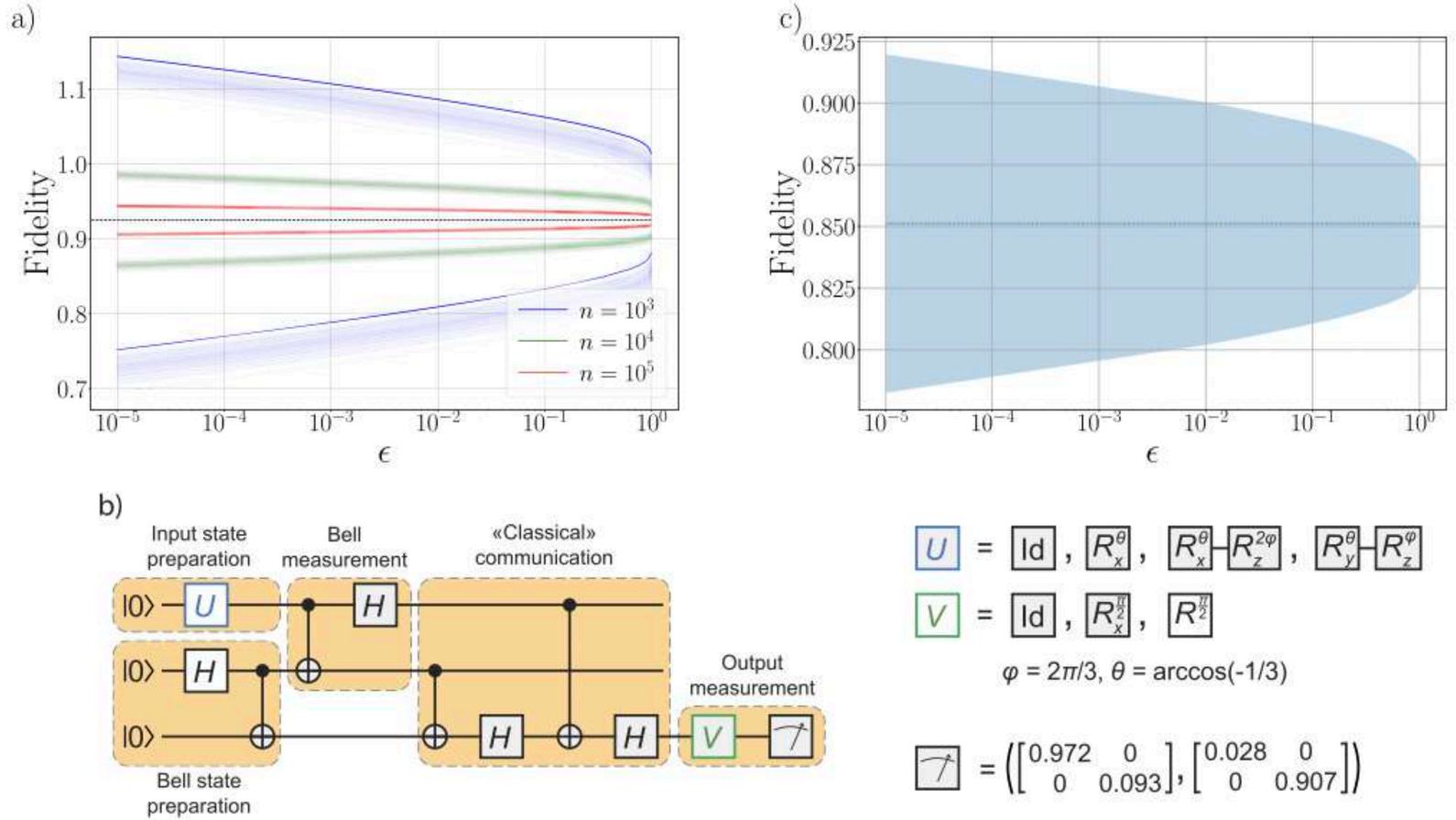

Figure 3. In (a) distribution of fidelity confidence intervals as the function of (one minus) CL over 100 numerical experiments for depolarizing channel and different values of n is shown. The single confidence interval for $n = 10^3$ is highlighted. The dashed line shows the true value of the fidelity. In (b) the circuit of the QPT protocol for the quantum teleportation channel is depicted (standard notations for Hadamard gate, controlled-NOT gate, and computational basis readout measurement are used). Gates U and V consistently take forms shown in the right-hand side, where $R^{\bullet}_{x(y)}$ is the standard rotation around $x(y)$ axis of the Bloch sphere (12 configurations of the circuit is run in total). The imperfections of readout computational basis measurement are also taken into account. In (c) the resulting fidelity confidence intervals for the QPT experiment from (b) run on IBM quantum experience superconducting processor is demonstrated. The dash line shows fidelity of the reconstructed point estimate of the channel.

Alternative quantum computing platforms

Progress in developing qudit-based processors

A universal qudit quantum processor with trapped ions

Martin Ringbauer,[1] Michael Meth,[1] Lukas Postler,[1] Roman Stricker,[1] Rainer Blatt,[1,2,3] Philipp Schindler,[1] and Thomas Monz[1,3]

[1] *Institut für Experimentalphysik, Universität Innsbruck, Technikerstrasse 25, 6020 Innsbruck, Austria*
[2] *Institut für Quantenoptik und Quanteninformation, Österreichische Akademie der Wissenschaften, Otto-Hittmair-Platz 1, 6020 Innsbruck, Austria*
[3] *Alpine Quantum Technologies GmbH, 6020 Innsbruck, Austria*

Today's quantum computers operate with a binary encoding that is the quantum analog of classical bits. Yet, the underlying quantum hardware consists of information carriers that are not necessarily binary, but typically exhibit a rich multilevel structure, which is artificially restricted to two dimensions. A wide range of applications from quantum chemistry to quantum simulation, on the other hand, would benefit from access to higher-dimensional Hilbert spaces, which conventional quantum computers can only emulate. Here we demonstrate a universal qudit quantum processor using trapped ions with a local Hilbert space dimension of up to 7. With a performance similar to qubit quantum processors, this approach enables native simulation of high-dimensional quantum systems, as well as more efficient implementation of qubit-based algorithms.

d=7
Trapped ions

Beyond Qubits: Unlocking the Third State in Quantum Processors

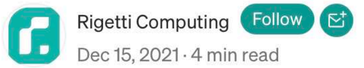

By Alex Hill, Senior Quantum Systems Engineer

d=3
Superconducting circuits

Results of 2020-2021: Qudit-based processor @ Lebedev Institute and RQC

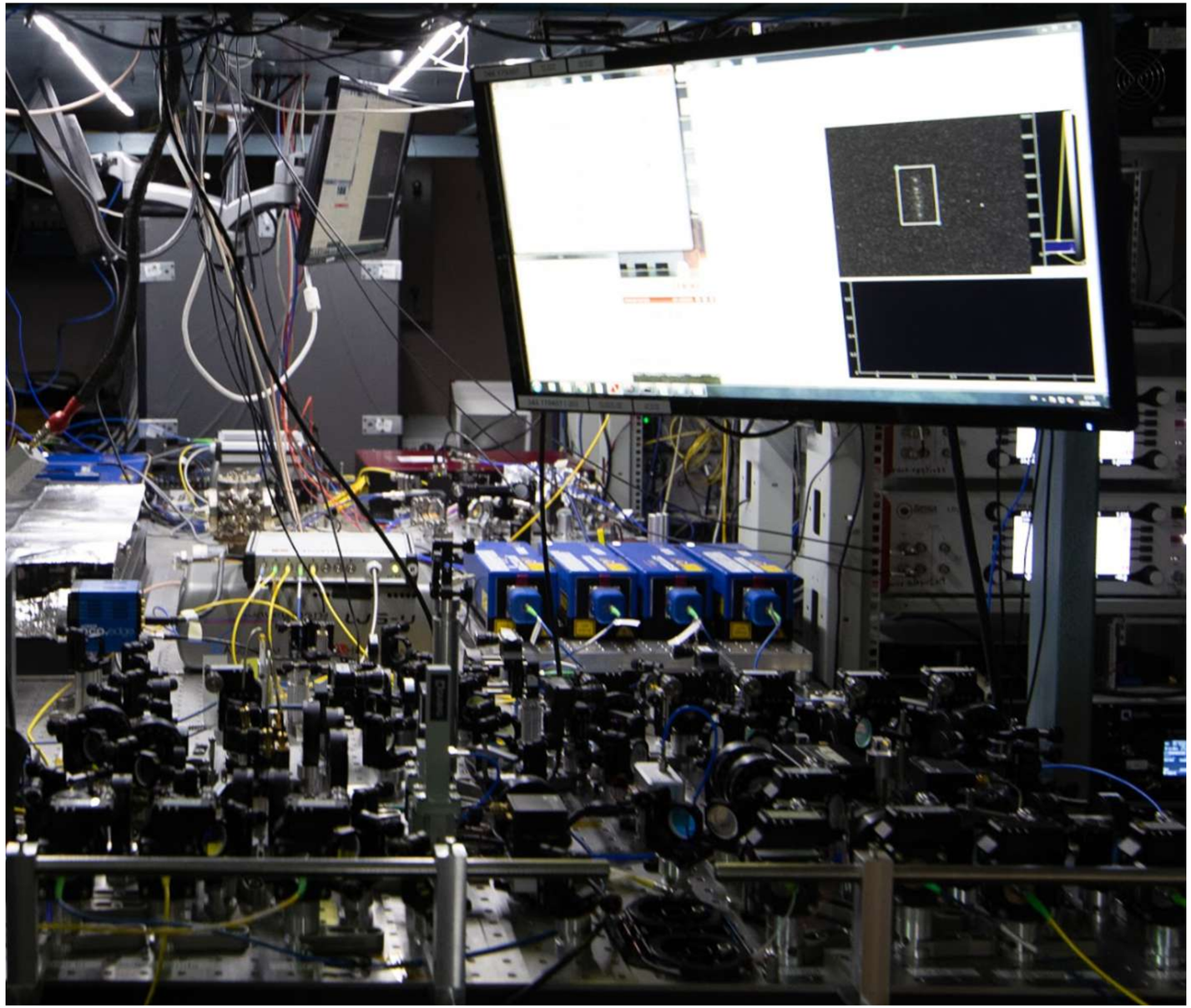

Qudit-based compiler

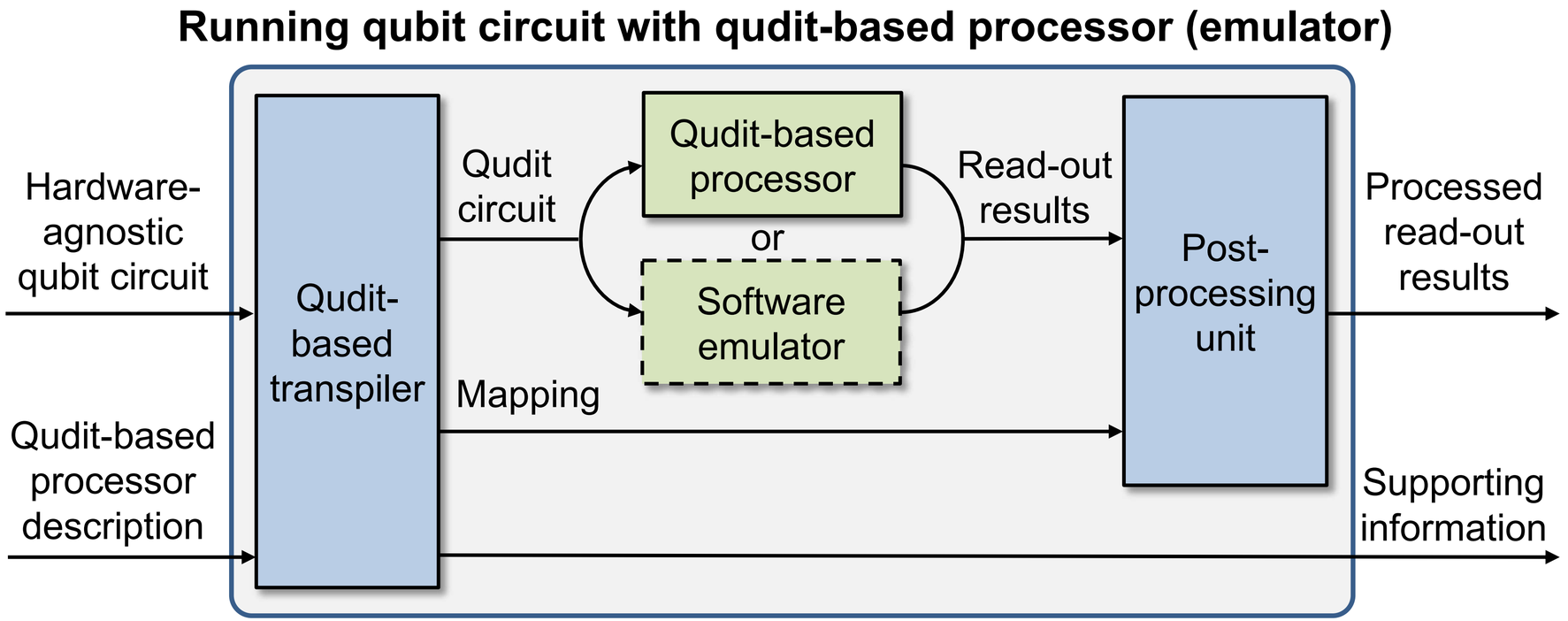

1) Maximizing the total fidelity:
2) Brute-force search for small-scale circuits;
3) Approximate search for more complicated situations (finding not the optimal, but better decompositions)

$$\mathcal{F}(\phi) = \prod_{i=1}^{D(\phi)} \left(1 - e_{\text{est}}(U_i^{\text{qd}}(\phi))\right),$$

A.S. Nikolaeva, E.O. Kiktenko, and A.K. Fedorov, https://arxiv.org/abs/2111.04384

Qudit-based compiler: Example

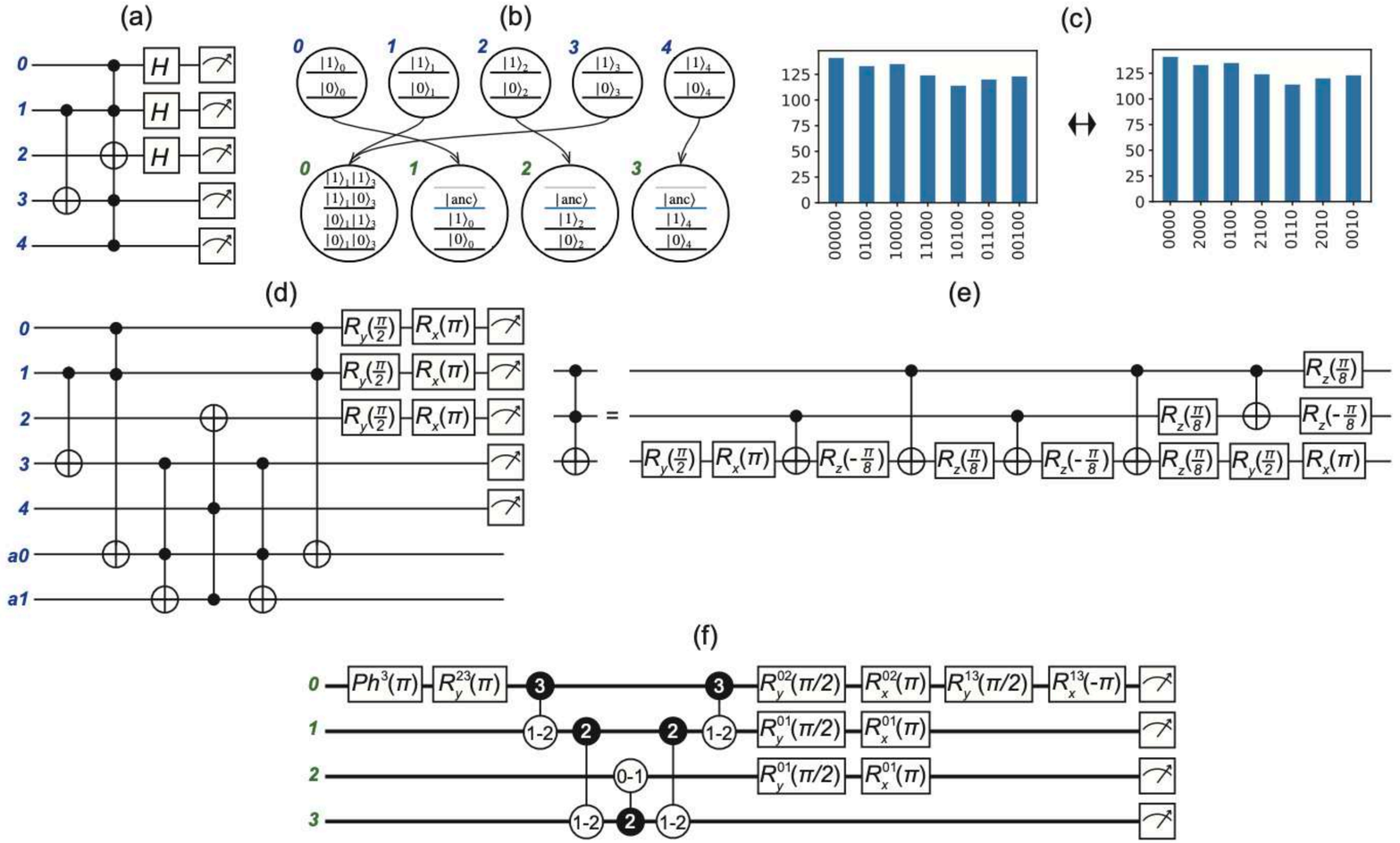

Figure 3. (a) Example of the input hardware-agnostic qubit circuit on $n = 5$ qubits (standard notations for CNOT, Hadamard gate, generalized Toffoli gate, and computational basis measurements are used). (b) Qubit-to-qudit mapping that is used for the realization of the given qubit circuit with $m = 4$ qudits and $d = 4$ levels. (c) Equivalence of read-out results that are obtained with qudit-based emulator and post-processed outputs, which can be interpreted as results of the circuit implementation. (d) Qubit-based transpilation for the input qubit circuit down to single-qubit gates and Toffoli gates. (e) Qubit-based transpilation for the Toffoli gate down to CNOT and single-qubit gates. (f) Qubit-based transpilation for the input qubit circuit down to the basic single-qudit and two-qudit generalized controlled gates (see Fig. 2a for the possibilities of the further transpilation).

Qubit-based decomposition: **31 two-qubit gates**.

Qudit-based decomposition: **5 two-qudit gates**.

Results of 2020-2021: LRC

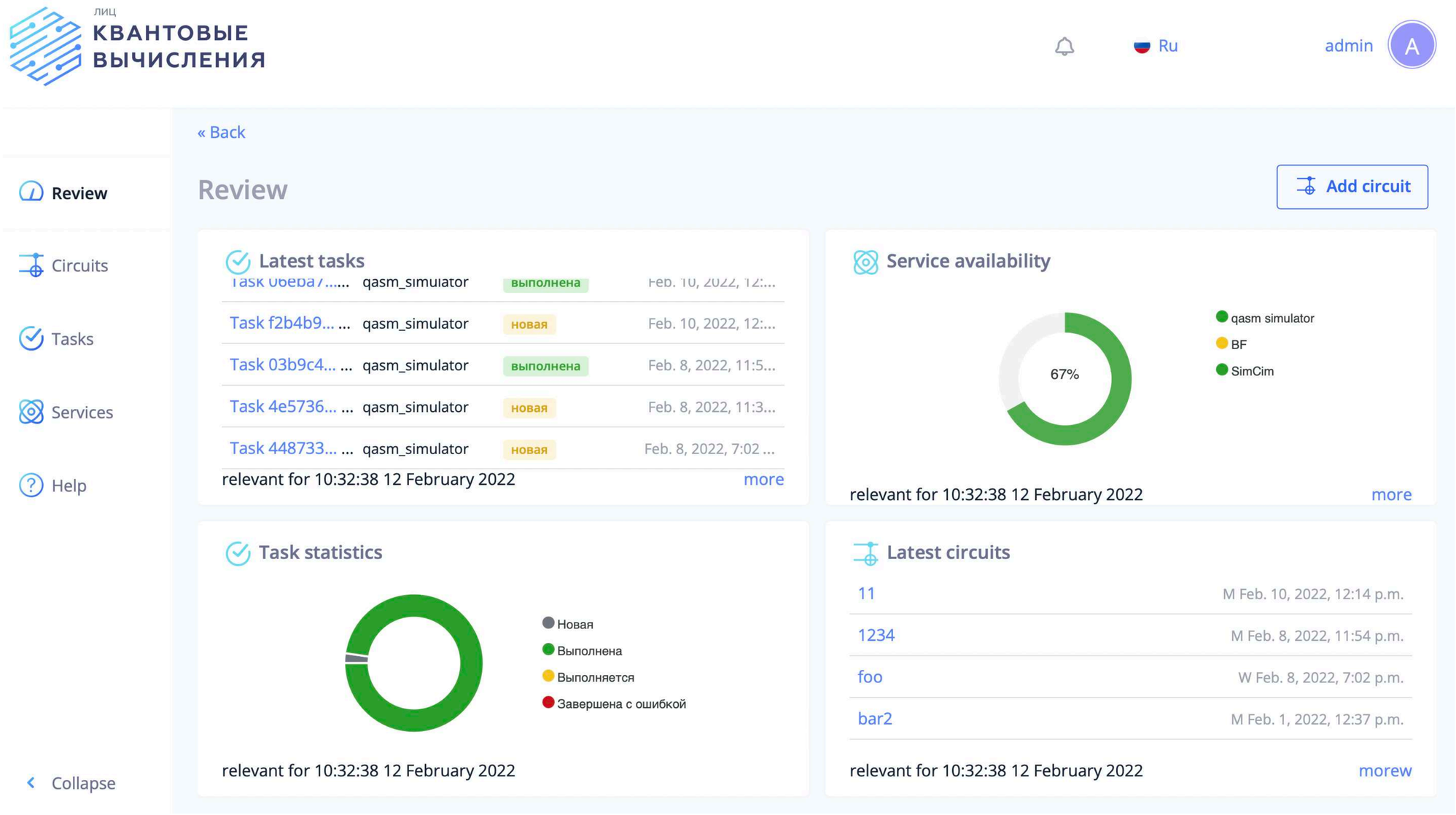

https://lrc-quantum.ru/login

Thank you for your attention!

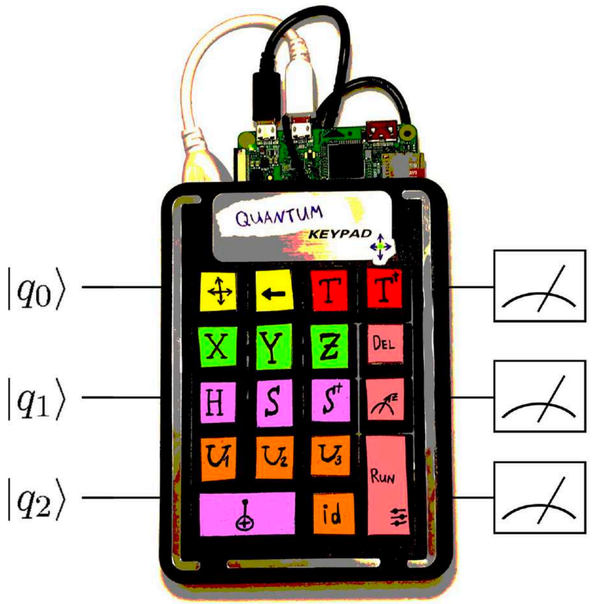

Invitation to publish in EPJ QT

Quantum computing: Brief history

Irreversibility and Heat Generation in the Computing Process

The Thermodynamics of Computation—a Review

Charles H. Bennett

IBM Watson Research Center, Yorktown Heights, New York 10598

Received May 8, 1981

Logical Reversibility of Computation*

Quantum Mechanical Computers[1]

Richard P. Feynman[2]

1. INTRODUCTION

This work is a part of an effort to analyze the physical limitations of computers due to the laws of physics. For example, Bennett(1) has made a careful study of the free energy dissipation that must accompany computation. He found it to be virtually zero. He suggested to me the question of the limitations due to quantum mechanics and the uncertainty principle. I have found that, aside from the obvious limitation to size if the working parts are to be made of atoms, there is no fundamental limit from these sources either.

Ю. И. МАНИН

ВЫЧИСЛИМОЕ И НЕВЫЧИСЛИМОЕ

Quantum Mechanical Hamiltonian Models of Turing Machines

Paul Benioff[1]

Simulating Physics with Computers

Richard P. Feynman

Department of Physics, California Institute of Technology, Pasadena, California 91107

Received May 7, 1981

Quantum theory, the Church–Turing principle and the universal quantum computer

BY D. DEUTSCH

Department of Astrophysics, South Parks Road, Oxford OX1 3RQ, U.K.

(*Communicated by R. Penrose, F.R.S. – Received* 13 *July* 1984)

VOLUME 48, NUMBER 4 PHYSICAL REVIEW LETTERS 25 JANUARY 1982

Is There a Fundamental Bound on the Rate at Which Information Can Be Processed?

David Deutsch

Astrophysics Department, Oxford University, Oxford OX1 3RQ, England, and Center for Theoretical Physics, University of Texas at Austin, Austin, Texas 78712

(Received 29 September 1981)

It is shown that the laws of physics impose no fundamental bound on the rate at which information can be processed. Recent claims that quantum effects impose such bounds are discussed and shown to be erroneous.

RESEARCH ARTICLES

Universal Quantum Simulators

Seth Lloyd

Feynman's 1982 conjecture, that quantum computers can be programmed to simulate any local quantum system, is shown to be correct.

Error correction codes: Shor's code

Structure for the Shor's code

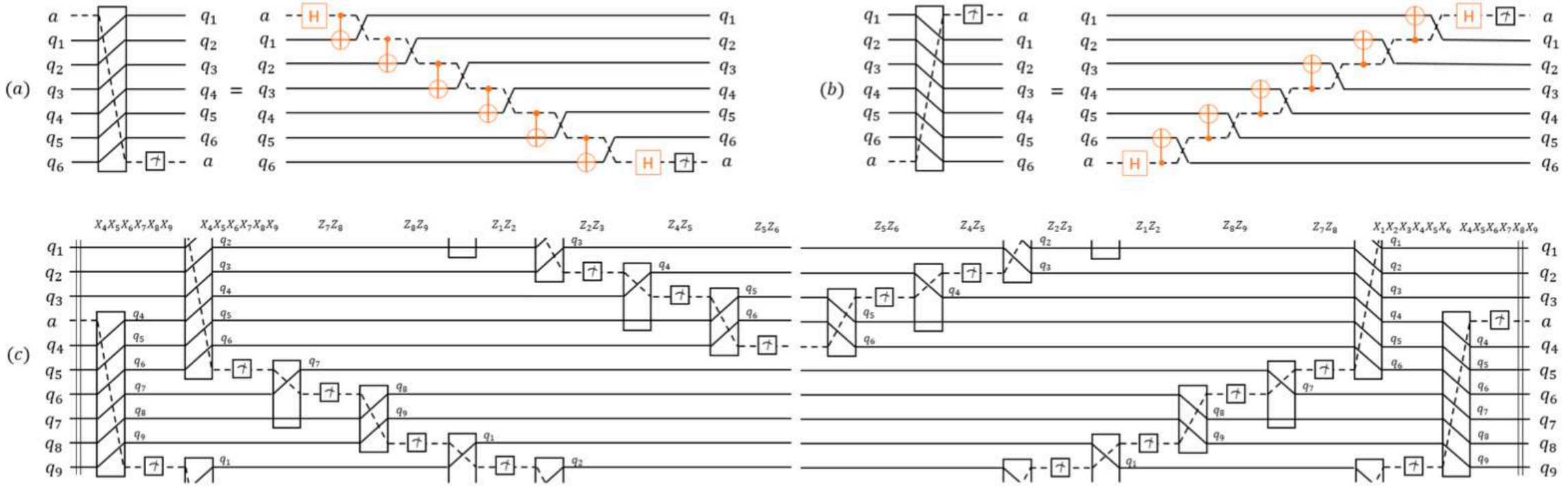

Probing non-Markovian dynamics

Probing non-Markovian dynamics: General scheme

Estimated from experimental data

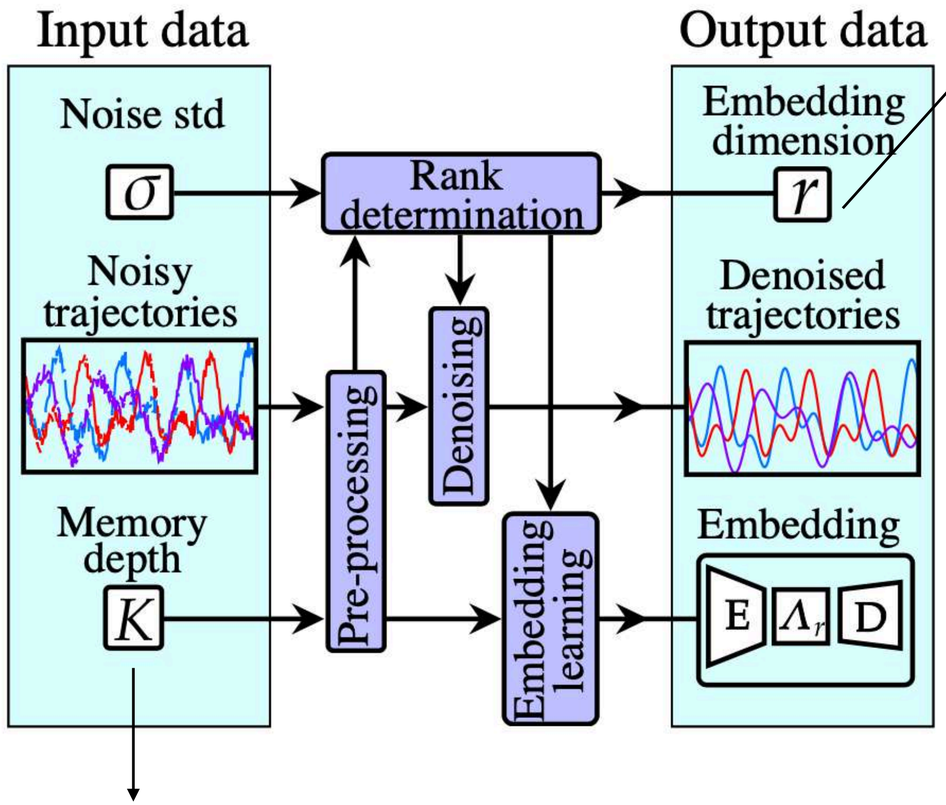

K is usually set knowingly large in order to capture all memory effects

We use *r*-dimensional Markovian embedding as follows (*r* is minimal dimension that provides a proper description of the considered dynamics):

Markovian embedding

Complex diagonal matrix that drives the Markovian dynamics of the embedding

$$\begin{cases} s(k+1) = \Lambda_r s(k), \\ \varrho(k) = \mathbf{D}[s(k)], \end{cases}$$

$$s(k) = \mathbf{E}[\varrho(k), \varrho(k-1), \ldots, \varrho(k-K+1)],$$

'Decoding' linear map reconstructing the density matrix from the corresponding embedding

r allows revealing an effective number of unknown degrees of freedoms, which are necessary to be taken into account in order to predict the state of the system; "Measure" of non-Markovianity and complexity of simulating dynamics of an open quantum systems

Probing non-Markovian dynamics: General scheme

Reconstructed Markovian embedding can be used for predicting the non-Markovian dynamics of the system, given a sequence of states at the first K time steps

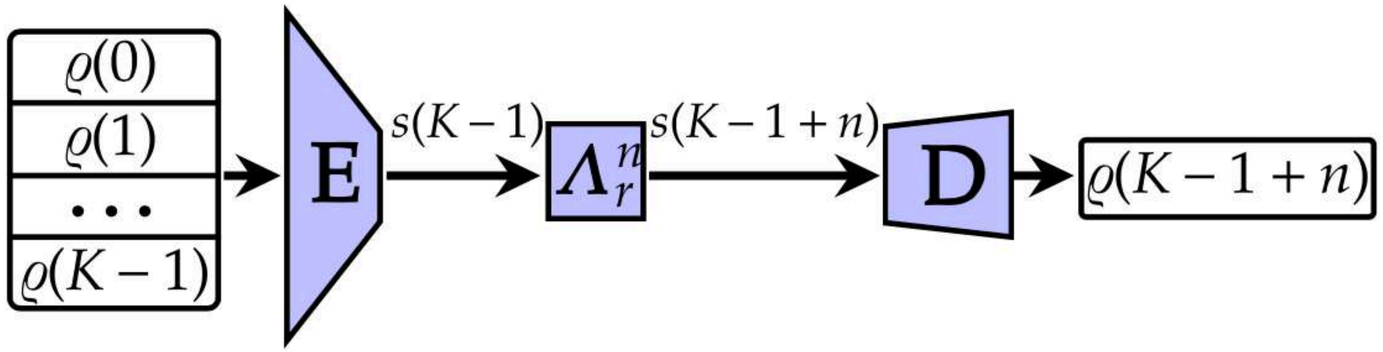

$$\varrho(K+n-1) = \mathbf{D}\left[\Lambda_r^n \mathbf{E}[\varrho(K-1), \varrho(K-2), \ldots, \varrho(0)]\right].$$

Probing non-Markovian dynamics: General scheme

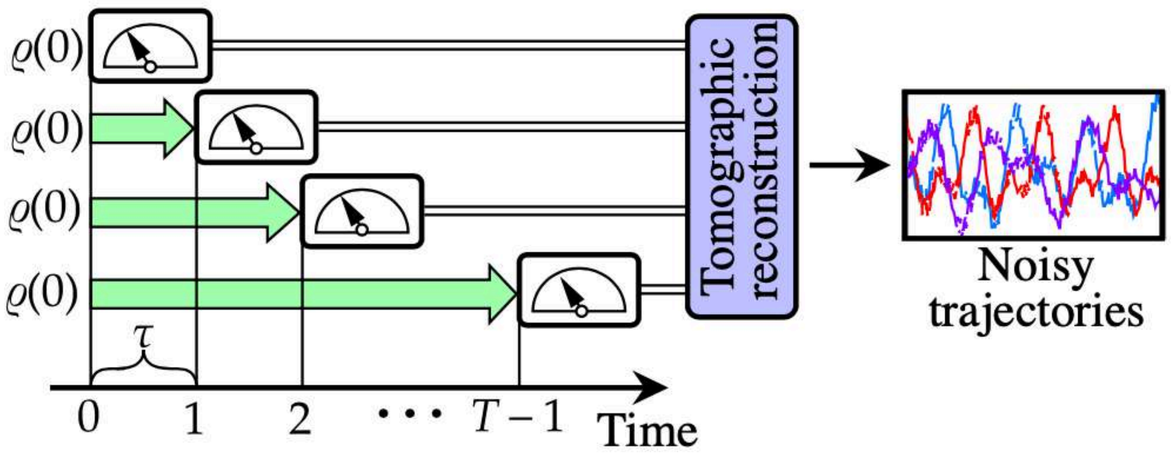

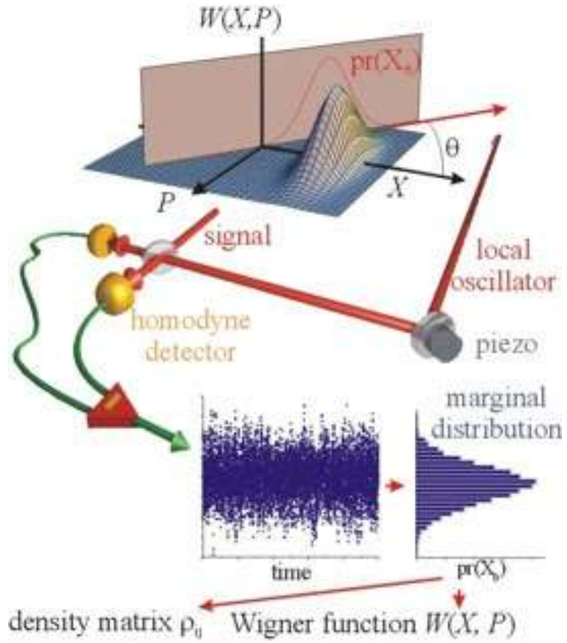

$(\varrho(0), \varrho(1), \ldots)$ system's trajectories: Input data for our analysis

$\varrho(k+1)$ depends on the whole prehistory $(\varrho(k), \varrho(k-1), \ldots)$

Quantum trajectories are irregular and challenging
for further analysis even in the case of low-dimensional systems

Probing non-Markovian dynamics: General scheme

Estimated from experimental data

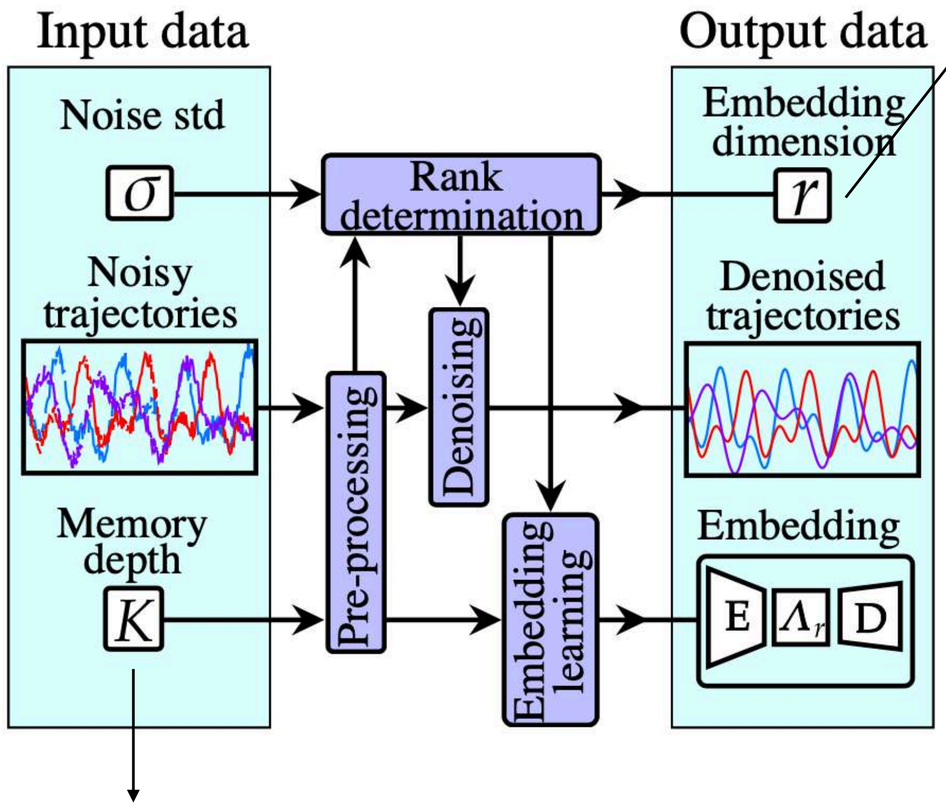

K is usually set knowingly large in order to capture all memory effects

r allows revealing an effective number of unknown degrees of freedoms, which are necessary to be taken into account in order to predict the state of the system.

The concept of the effective dimension of the environment: the minimal possible dimension of the environment that reproduces the same non-Markovian dynamics of the system:

$$d_{\mathrm{E}}^{\mathrm{eff}} = \left\lceil \sqrt{r/d^2} \right\rceil$$

“Measure" of non-Markovianity and complexity of simulating dynamics of an open quantum systems

Dimensionality of the system

Details of the approach: Nakajima-Zwanzig equation and Markovian embedding

Discrete time version of the Nakajima-Zwanzig equation:

$$\varrho(k+1) = \sum_{i=1}^{K} \mathcal{M}_i[\varrho(k-K+i)], \quad k \in \{K-1, K, \ldots\},$$

Vectorized form:

$$|\varrho(k+1)\rangle\rangle = M \begin{bmatrix} |\varrho(k-K+1)\rangle\rangle \\ \vdots \\ |\varrho(k)\rangle\rangle \end{bmatrix}, \quad M := \begin{bmatrix} M_1 & \ldots & M_K \end{bmatrix}, \qquad |i\rangle\langle j| \mapsto |i\rangle \otimes |j\rangle$$

Nakajima-Zwanzig equation and a Markovian embedding:

$$R(k+1) = \overline{M} R(k), \quad R(k) := \begin{bmatrix} |\varrho(k-K+1)\rangle\rangle \\ \vdots \\ |\varrho(k)\rangle\rangle \end{bmatrix} \qquad \overline{M} := \left[\begin{array}{ccc|ccc} 0 & \ldots & 0 & 1 & \ldots & 0 \\ \vdots & \ddots & \vdots & \vdots & \ddots & \vdots \\ 0 & \ldots & 0 & 0 & \ldots & 1 \\ \hline \multicolumn{6}{c}{M} \end{array}\right],$$

Reinforcement learning: Partially observed environment

Details of the approach: Nakajima-Zwanzig equation and Markovian embedding

Nakajima-Zwanzig equation and a Markovian embedding:

$$R(k+1) = \overline{M} R(k), \quad R(k) := \begin{bmatrix} |\varrho(k-K+1)\rangle\rangle \\ \vdots \\ |\varrho(k)\rangle\rangle \end{bmatrix} \qquad \overline{M} := \begin{bmatrix} 0 & \dots & 0 & 1 & \dots & 0 \\ \vdots & \ddots & \vdots & \vdots & \ddots & \vdots \\ 0 & \dots & 0 & 0 & \dots & 1 \\ \hline & & & M & & \end{bmatrix},$$

$Kd^2 \times Kd^2$; $d^2(K-1) \times d^2$; $(K-1)d^2 \times (K-1)d^2$

if we consider R(k) as the state of some new abstract system at a discrete time moment k, then the next state R(k+1) depends only on R(k) and the time-independent dynamics generator M. All these states belong to some r-dimensional subspace ***R***, where r can be less than Kd^2. This fact can be used to reduce the dimension.

$$R(k+1) = \overline{M} R(k) \longrightarrow R(k+1) = \overline{M} \pi_{\mathcal{R}} R(k),$$

where $\pi_{\mathcal{R}}$ is the orthogonal projection matrix on the subspace $\mathcal{R}$

Physical trajectories

Eigendecomposition:

$$\overline{M}\pi_{\mathcal{R}} = Q^{-1}\Lambda Q,$$

only r leading eigenvalues from Λ are non-zero.

Truncation:

$$D := Q^{-1}[:, :r], \quad E := Q[:r, :], \quad \Lambda_r := \Lambda[:r, :r],$$

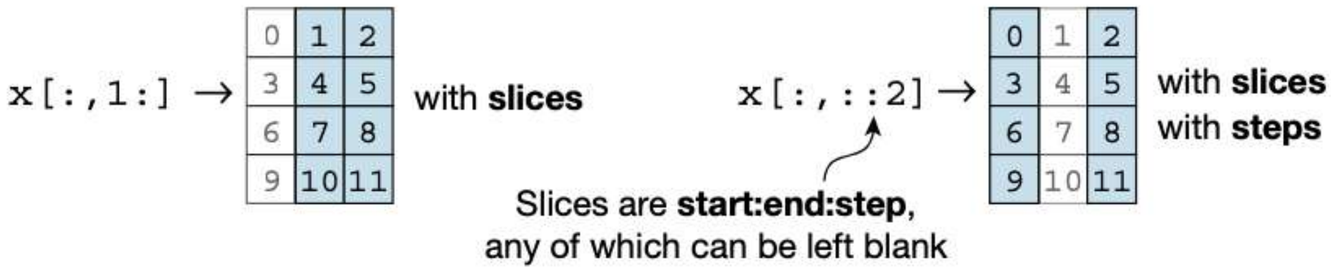

Details of the approach

The truncated eigendecomposition allows compressing R(k)

$$R(k+n) = D\Lambda_r^n E\ R(k).$$

Alternatively:

Encoding

$$s(k) = ER(k),$$

Decoding

$$R(k) = Ds(k),$$

Embedding evolution

$$s(k+1) = \Lambda_r s(k).$$

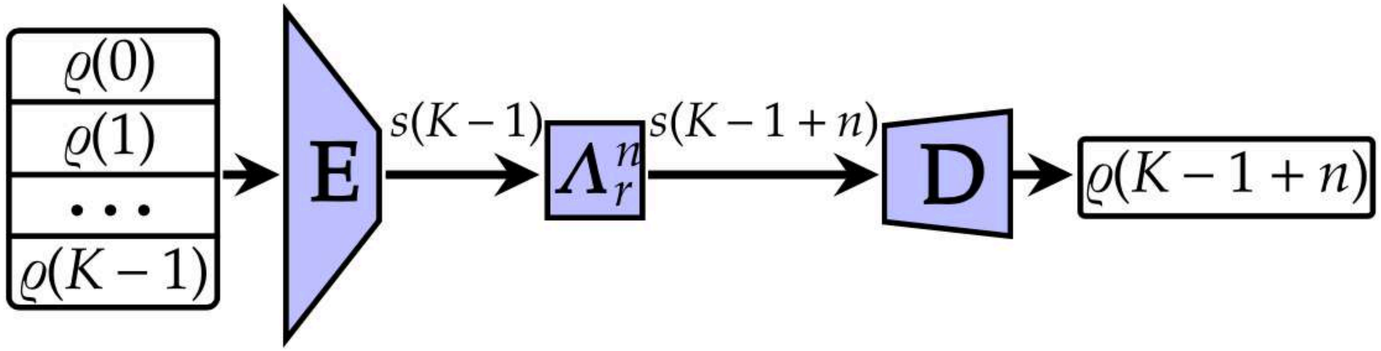

Data processing within the Markovian embedding reconstruction

Initial data:

$$\mathcal{S}_{\text{noisy}} = \{\mathcal{T}^{(1)}_{\text{noisv}}, \mathcal{T}^{(2)}_{\text{noisv}} \ldots, \mathcal{T}^{(L)}_{\text{noisv}}\}$$

$$\mathcal{T}^{(i)}_{\text{noisy}} = \left(\varrho^{(i)}_{\text{noisy}}(0), \varrho^{(i)}_{\text{noisy}}(1), \ldots, \varrho^{(i)}_{\text{noisy}}(T-1)\right)$$

Memory depth hyper-parameter (K)

Noise std

Output:

the minimal Markovian embedding dimension (r)

$D,\ E,\ \Lambda_r$ (dynamics)

+

Denoised trajectories

Data processing within the Markovian embedding reconstruction

We construct three auxiliary matrices:

$$H^{(i)}_{\text{noisy}} = \begin{bmatrix} |\varrho^{(i)}_{\text{noisy}}(0)\rangle\rangle & |\varrho^{(i)}_{\text{noisy}}(1)\rangle\rangle & \dots & |\varrho^{(i)}_{\text{noisy}}(T-K+1)\rangle\rangle \\ |\varrho^{(i)}_{\text{noisy}}(1)\rangle\rangle & |\varrho^{(i)}_{\text{noisy}}(2)\rangle\rangle & \dots & |\varrho^{(i)}_{\text{noisy}}(T-K+2)\rangle\rangle \\ \vdots & \vdots & \ddots & \vdots \\ |\varrho^{(i)}_{\text{noisy}}(K-1)\rangle\rangle & |\varrho^{(i)}_{\text{noisy}}(K)\rangle\rangle & \dots & |\varrho^{(i)}_{\text{noisy}}(T)\rangle\rangle \end{bmatrix},$$

$$X^{(i)}_{\text{noisy}} = H^{(i)}_{\text{noisy}}[:, :-1], \quad Y^{(i)}_{\text{noisy}} = H^{(i)}_{\text{noisy}}[:, 1:],$$

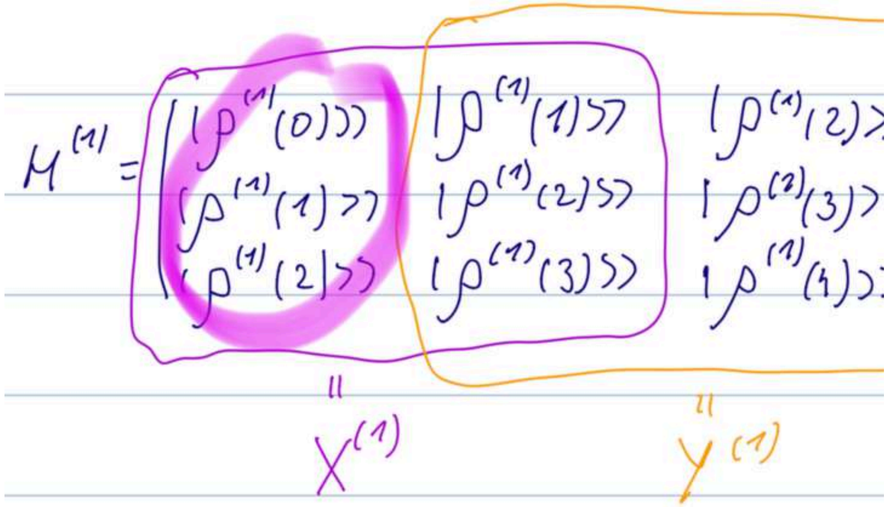

X and Y are shifted one step relative to each other

Then we stack matrices within sets of multiple trajectories:

$$X_{\text{noisy}} = \begin{bmatrix} X^{(1)}_{\text{noisy}} & X^{(2)}_{\text{noisy}} & \dots & X^{(L)}_{\text{noisy}} \end{bmatrix},$$

$$Y_{\text{noisy}} = \begin{bmatrix} Y^{(1)}_{\text{noisy}} & Y^{(2)}_{\text{noisy}} & \dots & Y^{(L)}_{\text{noisy}} \end{bmatrix},$$

$$H_{\text{noisy}} = \begin{bmatrix} H^{(1)}_{\text{noisy}} & H^{(2)}_{\text{noisy}} & \dots & H^{(L)}_{\text{noisy}} \end{bmatrix}.$$

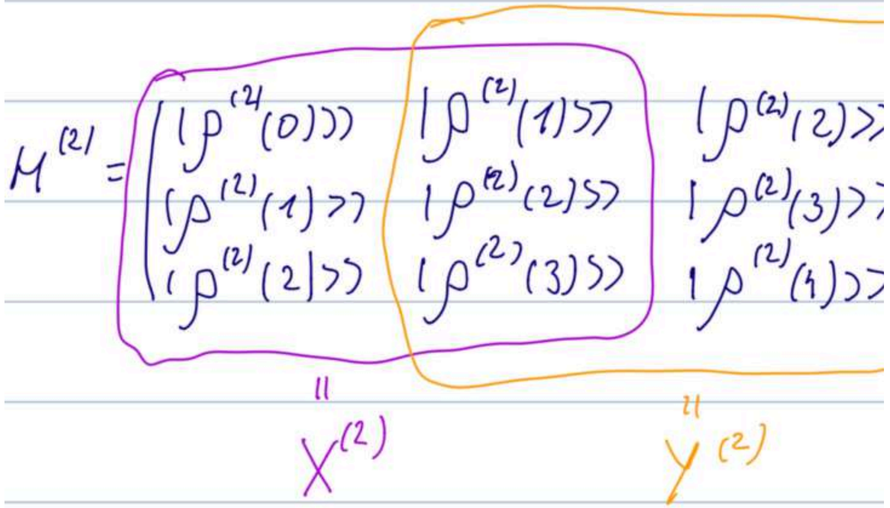

Data processing within the Markovian embedding reconstruction

We introduce a low-rank approximation and then recast it back into the set of trajectories. The optimal approximation of H_noisy can be obtained using singular value decomposition (SVD):

$$H_\eta = U[:, :\eta] S[:\eta, :\eta] V[:, :\eta]^\dagger,$$

The optimal rank than leads to the best denoising of a matrix without significant states distortion can be estimated by using the method of Gavish and Donoho (2014):

$$\eta_{\text{opt}} = \sum_i \text{trunc}_\sigma(S[i,i]),$$

$$\text{trunc}_\sigma(x) = \begin{cases} 1, & x \geq \sigma\sqrt{2}\sqrt{n} f\left(\frac{m}{n}\right), \\ 0, & \text{otherwise}, \end{cases}$$

$$f(\beta) = \sqrt{2(\beta+1) + \frac{8\beta}{(\beta+1) + \sqrt{\beta^2 + 14\beta + 1}}},$$

$$H_{\text{denoised}} = H_{\eta_{\text{opt}}}.$$

$$r = \eta_{\text{opt}}.$$

Data processing within the Markovian embedding reconstruction

Denoised versions:

$$X_{\text{denoised}} = U[:, : \eta_{\text{opt}}]U[:, : \eta_{\text{opt}}]^{\dagger} X_{\text{noisy}},$$
$$Y_{\text{denoised}} = U[:, : \eta_{\text{opt}}]U[:, : \eta_{\text{opt}}]^{\dagger} Y_{\text{noisy}}.$$

Minimization wrt to Frobenius norm:

$$\overline{M} = \underset{W}{\operatorname{argmin}} \| Y_{\text{denoised}} - W X_{\text{denoised}} \|_{\text{F}},$$

Optimal-rank solution:

$$\overline{M}_{\eta_{\text{opt}}} = Y_{\text{denoised}} X^{+}_{\text{denoised}},$$

Reconstructing encoding and decoding matrices from M:

$$\overline{M}\pi_{\mathcal{R}} = Q^{-1}\Lambda Q,$$

$$D := Q^{-1}[:, : r], \quad E := Q[: r, :], \quad \Lambda_r := \Lambda[: r, : r],$$

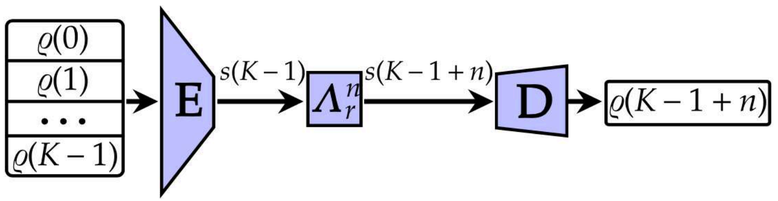

Dynamics prediction is possible!

Predicted Markovian embedding minimal dimension

Qubit with a finite dimensional environment; we sample at random a quantum dynamical semigroup generator in the GKSL form. We simulate noise appearing during data acquisition of trajectories.

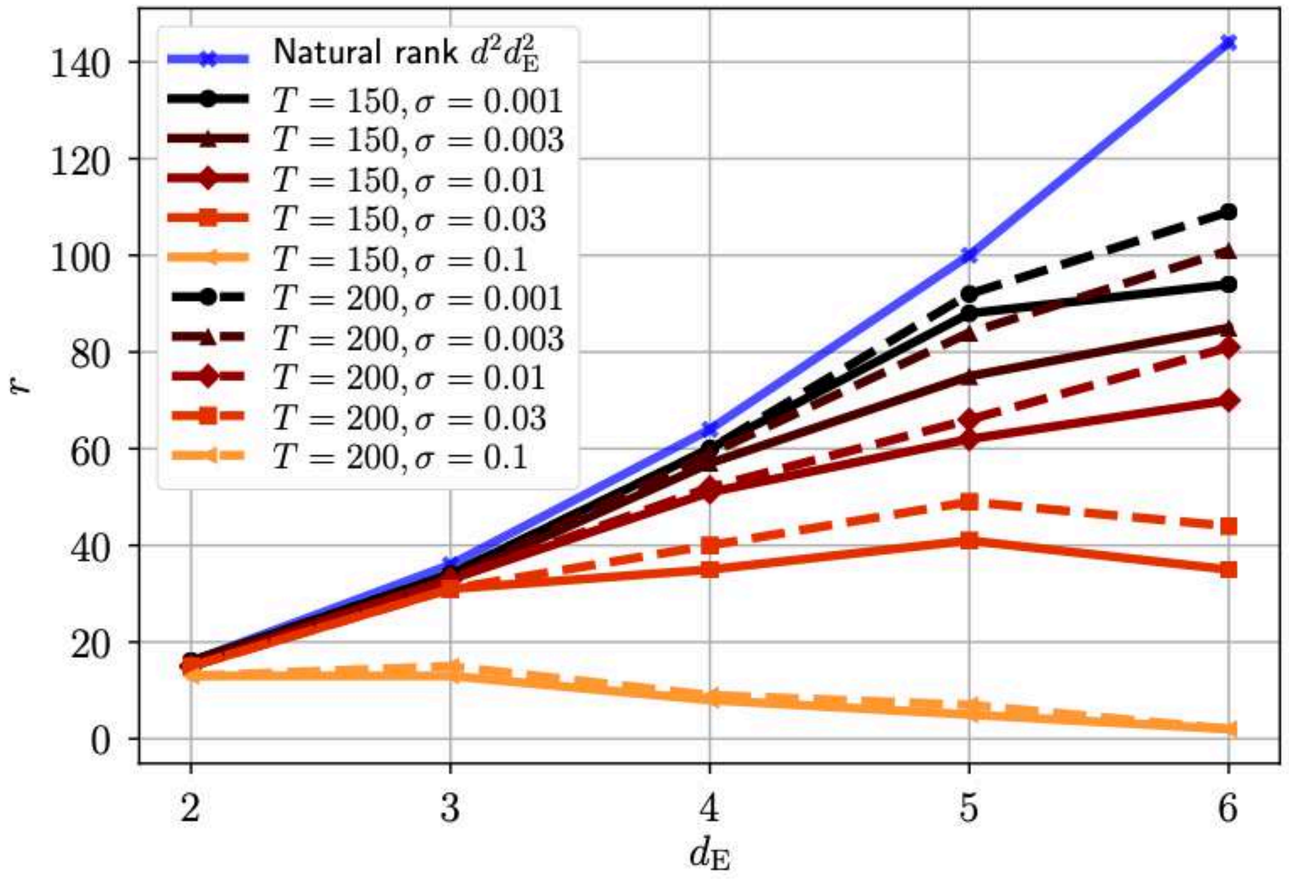

The method works correctly and predicts the irregular non-Markovian dynamics of a qubit

Selection of the memory depth hyperparemeter

Qubit with a finite dimensional environment; we sample at random a quantum dynamical semigroup generator in the GKSL form. We simulate noise appearing during data acquisition of trajectories.

$$\mathcal{D}^{\mathrm{test}}(\mathcal{T}_1, \mathcal{T}_2) = \frac{1}{T-K} \sum_{k=K}^{T-1} \|\varrho_1(k) - \varrho_2(k)\|_1,$$

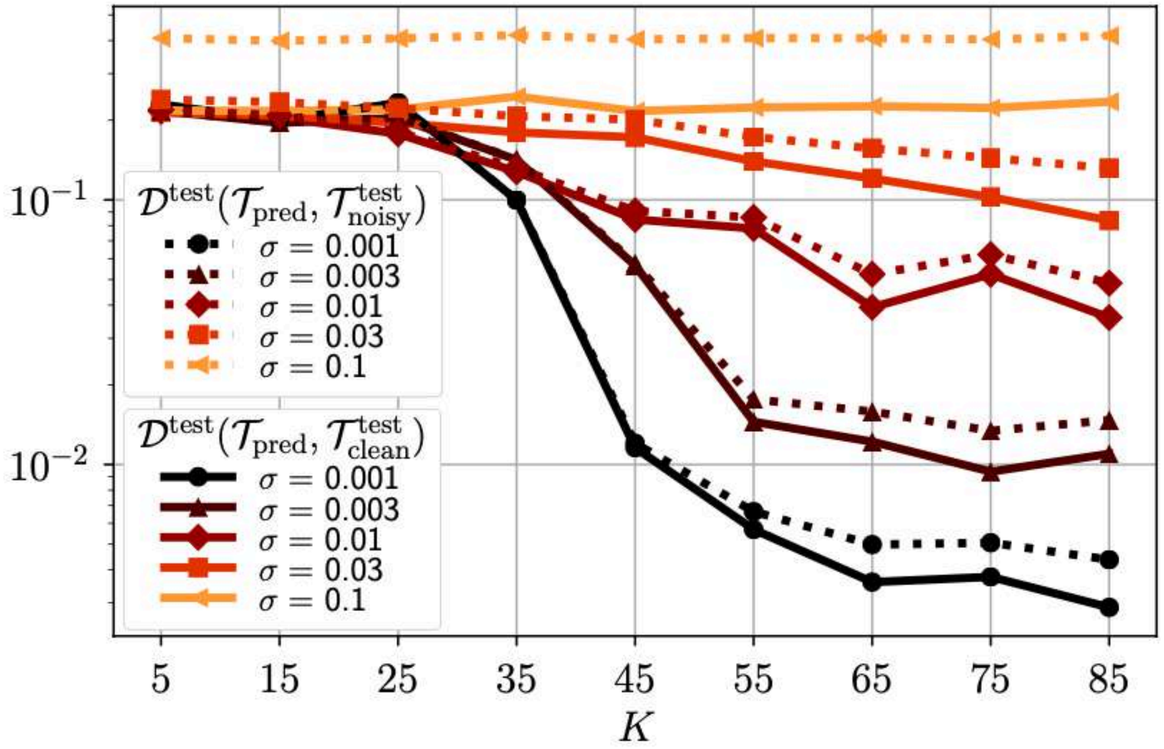

‘Saturation’ value of K: starting from which the accuracy of prediction is mainly determined by the noise level

Quality of deniosing

Qubit with a finite dimensional environment; we sample at random a quantum dynamical semigroup generator in the GKSL form. We simulate noise appearing during data acquisition of trajectories.

$$\mathcal{D}(\mathcal{S}_1, \mathcal{S}_2) = \frac{1}{LT} \sum_{l=1}^{L} \sum_{k=0}^{T-1} \|\varrho_1^{(l)}(k) - \varrho_2^{(l)}(k)\|_1,$$

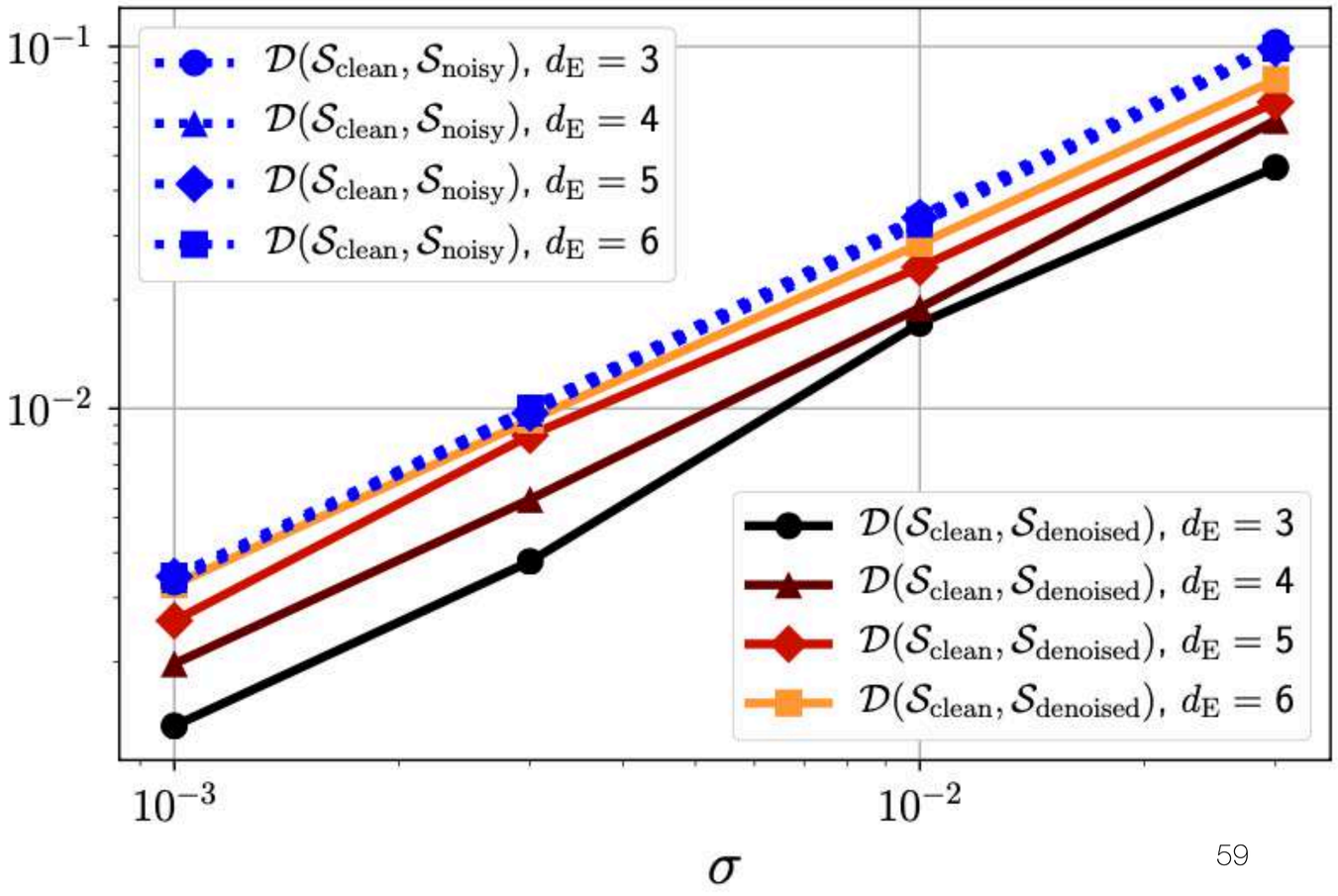

As a valuable by-product of the rank estimation we obtain the denoised version of a data set.

Reconstructing eigenfrequencies of the joint system

Qubit with a finite dimensional environment; we sample at random a quantum dynamical semigroup generator in the GKSL form. We simulate noise appearing during data acquisition of trajectories. A comparison of the spectrum of the quantum channel exp(τL) driving the dynamics of the joint system and environment density matrix with the diagonal elements of Λ_r

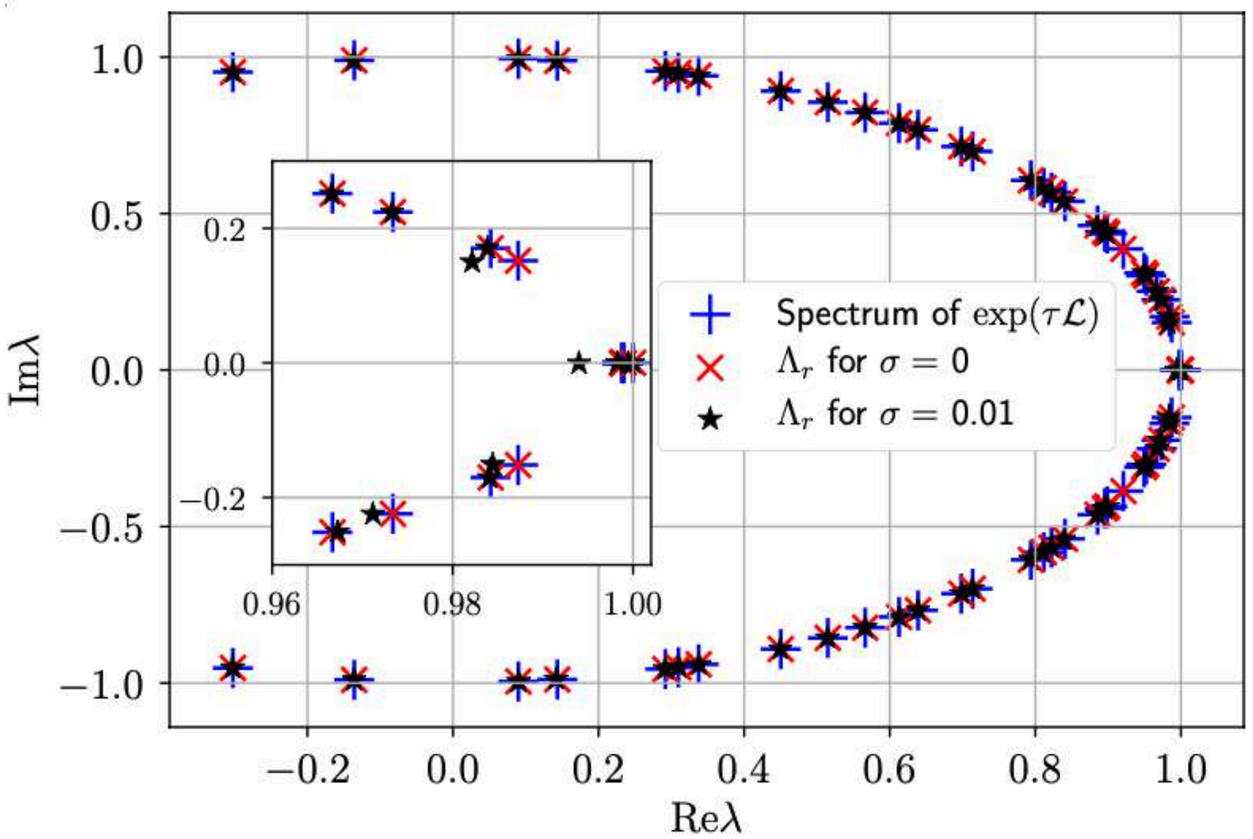

A perfect coincidence in the case without noise; in the presence of noise, we see that the approach provides valuable information about eigenfrequencies.